Differential Millimetre Wave On-Chip Inductors

FRANCISCO GONZÁLEZ MAÑERO
MASTER´S THESIS
DEPARTMENT OF ELECTRICAL AND INFORMATION TECHNOLOGY
FACULTY OF ENGINEERING | LTH | LUND UNIVERSITY

Differential Millimetre Wave On-Chip Inductors

Francisco González Mañero
fr4442go-s@student.lu.se

Department of Electrical and Information Technology
Lund University

Supervisor:
Lars Ohlsson Fhager
Stefan Andric

Examiner:
Pietro Andreani

September 16, 2019

Printed in Sweden
Tryckeriet i E-huset, Lund

Abstract

The increasingly interconnected world requires systems that support high data rates, and thus the development of mm-wave systems is necessary. Automotive collision radar (80 GHz) or WLANs (60 GHz) are one of the applications that led the increment of the demand in RFICs, in which monolithic devices are fundamental, such as on-chip inductors or transformers. Along this thesis, the design and modelling of single and differential inductors, as well as transformers, are carried out following a bottom-to-top structure. Electromagnetic Momentum μW ADS simulations characterize the inductors and transmission line-based lumped-element equivalent models of the inductors and transformers are also defined. The exploration of the design of inductors in the custom-made technology available in the Nanoelectronics Group Student Design Library of Lund University is the main goal of the thesis. A close agreement between model and component is achieved, just as the design of inductors and transformers that can work over the desired band using the presented technology.

Popular Science Summary

The current exponential growth of the Earth population implies an increase in the information that is shared and stored. For that, not only high storage systems are needed but also higher transmission rates. The Extremely High Frequency (EHF) band or millimeter-wave band is defined as a part of the Radio Frequency (RF) spectrum that allows high data rates by having high bandwidth bands. This emerging mm-wave regime covers frequencies from 30 to 300 GHz in which different sub-bands can be defined, such as the well-known W-band used in this work.

Around the mid 2000s, the demand for low cost Radio Frequency Integrated Circuits (RFICs) increased, as well as the development of new modulation schemes for transceivers and receivers. In a transceiver/receiver diagram block, it is possible to notice that voltage controlled oscillators (VCO), low noise amplifiers (LNA) or impedance matching circuits are key blocks when it comes to transmission of data. One of the most important elements of those mentioned RFICs (VCO, LNA, impedance matching circuit) are, indeed, monolithic(on-chip) inductors. For that reason, a research of monolithic inductors design in an specific technology enables this technology to be suitable to develop RFICs that includes inductors, expanding its range of application.

Throughout this thesis, the suitability of a custom-made technology for the design of inductors is implemented. During the design process, not only electromagnetic simulations are done, but the description of lumped-element equivalent models as well. Single inductors are designed, but differential inductors and transformers too, providing a more complex description of the design. That may allow this work to be the start point for a inductor design kit that could be fully developed based on this document.

Table of Contents

List of Figures

List of Tables

Chapter 1

Introduction

In the communication age we live in, the number of devices and the need of communication between them are increasing notoriously [1]. In order to meet the needs, Radio Frequency Integrated Circuits (RFIC) have experienced an increase in their demand and big data exchanges have made necessary the development of high-data-rate systems, moving electronics evolution to millimeter-wave frequencies (30 – 300 GHz) [1]. Radars, security or wireless commercial applications (WiHD at 60 GHz, automotive collision radar at 77 GHz or imaging systems at 94 GHz) are only some examples of applications that contribute to the creation of a smart society in which everything is connected and communication between people is becoming easier and easier [2].

Passive on-chip inductors and transformers are key components in mm-wave RFICs since their inductance and quality factor impact overall circuit performance. This performance can be improved with the use of differential instead of a single inductors. Differential circuits show better noise rejection and robustness, which is essential in transceivers aimed for mm-wave communication [3].

The use of monolithic inductors is not exempt from difficulties. This type of inductor requires a large on-chip area, so the cost increases. Furthermore, several losses and parasitics that decreases inductor's Q-factor have to be taken into consideration, such as the substrate effect, the skin effect or the proximity effect [4]. Different ways of reducing the substrate losses in silicon-based technologies are shown in [4].

Not only passive inductors exists, but active inductors as well, formed by transistors or other active components [5]. Active inductors have some advantages over the passive inductors, such as area reduction, high frequency, high quality factor or large and tunable inductance [6]. However, active inductors have notorious limitations in respect of coupling, power consumption and design. They cannot be coupled (Their inductance is not created from the electromagnetic field around them), they have a higher power consumption and they require slower and more involved design process in comparison with their passive counterparts [7]. The choice between active or passive inductors depends on the application, so active inductors will be suitable for filters [5] [6] and passive inductors for circuits in which an energy transfer is needed (They can be coupled so they can form transformers). Some examples of RFICs where differential passive on-chip inductors are commonly used are voltage controlled oscillators (VCO), power amplifiers, low noise amplifiers (LNA), phase shifters or impedance matching circuits [4].

1.1 Aim and structure

The main goal of this thesis is modelling and characterizing on-chip differential inductors and transformers in the W-band (75 – 110 GHz) of the mm-wave regime using the *Keysight Advanced Design System* (ADS) software. The choice of the W-band is done because it is becoming more attractive to have communication standards at those frequencies and the III-V nanowire RF MOSFETs technology used is suitable to be utilized this band [8]. Additionally, due to relatively large bandwidth (BW), this frequency band allows for high data rates as well. The technology used here is a custom-made nanowire RF MOSFETs, complemented with back-end-of-line (BEOL). This technology is described and available in the Nanoelectronics Group Student Design Library of the Lund University [9], and it has already been proved to be suitable for microstrip measurements in the mm-wave regime [10].

In order to systematically analyze inductors and transformers of different configurations, the following tasks were considered.

- Design single-ended and differential on-chip inductors.
- Design on-chip transformers.
- Develop equivalent lumped-element models for inductors and transformers.
- Compare different variations on the shape of the inductors and transformers.
- Quantify inductance, resistance and Q-factor for different configurations, based on simulated data.
- Characterize the transformer insertion losses, frequency range, impedance ratio, coupling, windings' DC resistance, self-inductance and Q-factor, based on simulated data.

The structure of the document is divided into five chapters. **Chapter 2** describes the theoretical concepts needed to understand the thesis. Most of them are related to the electromagnetic fields that affects the inductor, but since the inductor structure will be based in transmission lines, parasitics, losses and other effects of the electromagnetic field in transmission lines are explained as well. **Chapter 3** presents the description of the inductors and all the measurements and the steps followed in order to obtain the results showed in the next chapter. **Chapter 4** shows the results obtained and their interpretation. In **Chapter 5**, final conclusions as well as future work is showed.

Chapter 2
Theoretical concepts

Along this chapter, a description of the theoretical concepts needed will be exposed. First, some basics of the inductor are shown and then several electromagnetic effects, parasitics, models and characteristics related to this inductor are presented. The final part is focused on the description of N-port networks and the measurements taken in this thesis.

It is common knowledge that circuits in general and RFICs in particular are composed of two main kind of components: active and passive components. Although it is necessary to have at least one active device in order to provide the circuit with energy, passive devices are often critical in RFICs such as power amplifiers or impedance matching circuits. Thus, this document will focus on one of the main passive elements, the inductor, and its characteristics.

2.1 Inductor

While active components provide power to the circuit, passive ones are responsible for maximizing power transfer through impedance matching. Some passive devices use the electromagnetic field around them to store and release energy, such as capacitors that store the energy in the electric field or inductors that use the magnetic field for that.

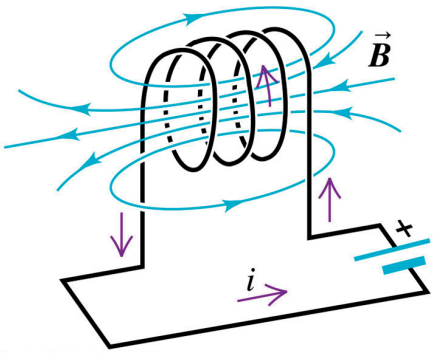

Figure 2.1: Magnetic flux density ($\vec{B}$) when a current (purple) is applied to the inductor [11]

Basically, an inductor consist of a wire that generates a magnetic field around it due to the current through it. Different materials and shapes can be used to make an inductor, but the most common structure is a wire wound into a coil, sometimes around a core. This structure shown in Figure 2.1 makes easy to store energy in the magnetic field since it is concentrated in the centre of the coil. However, it is not possible to directly fabricate such an inductor on-chip. A simple on-chip inductor can be formed from a transmission line stub (section 2.2), whose characteristics will be of interest since the inductors of this thesis are transmission line-based.

The main electrical measurement applied to an inductor is, as its name suggests, the inductance, that can be defined as the magnetic flux generated per unit of current [12]. In the case of the coil in Figure 2.1, it is possible to measure this inductance dividing the number of magnetic field line loops by the current in the wire. Since the magnetic field line loops unit is Weber, the units for inductance are Weber/Ampere or Henry.

Inductance can also be described as the relationship between the voltage in the inductor and the variation of the current through it as shown in the following equation

$$v(t) = L\frac{di(t)}{dt} \tag{2.1}$$

where L is the inductance in Henrys, v is the voltage in Volts and i is the current in Amperes.

Inductors can suffer external perturbations and its electromagnetic field can be changed because of the presence of nearby inductors or ground planes. Inductive coupling happens when a variation in the current through one inductor induces a voltage on the second inductor due to variations in the magnetic field. Then the two inductors are coupled and the way to measure it is the **mutual inductance**, defined as the relationship between the voltage in one inductor due to the variation of the current through other inductor. In this case, a wider definition of the inductance in equation 2.1 would be **self-inductance**, in equation 2.2, that relates variations in the current through one inductor with its own voltage [13].

$$v_1(t) = L_1\frac{di_1(t)}{dt} \tag{2.2}$$

$$v_2(t) = M_{21}\frac{di_1(t)}{dt} \tag{2.3}$$

where M_{12} is the mutual inductance and L_1 is the self-inductance, both in Henry. Sub-indexes 1 and 2 identify the two different inductors. Coupling can also be capacitive and it happens when two parallel plates (two inductors or an inductor and the ground plane) act like a capacitor.

Mutual inductance depends on how one inductor is affected by the magnetic field of a nearby inductor. The strength of this coupling can be modeled by the coupling coefficient $|k| < 1$, where $|k| = 1$ means that the inductors are totally coupled and $|k| = 0$ means that there is no coupling at all. Assuming then that the coupling characteristic is reciprocal it is possible to consider that mutual inductance is equal in both directions so $M_{12} = M_{21} = M$. In terms of L_1 and L_2, mutual

inductance between two inductors can be defined by equation 2.4 and shown in Figure 2.2.

$$M = k\sqrt{L_1 L_2} \tag{2.4}$$

The figure below shows the schematic used for transformers (section 2.1.1), where two coupled inductors are defined by their self-inductances and the coupling coefficient. That is because transformers are basically two coupled inductors.

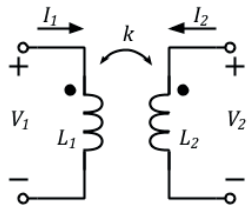

Figure 2.2: Two coupled inductors. L_1 and L_2 are the self-inductances of the inductors and k is the coupling coefficient.

As it will be explained in section 2.3, some different parasitics affect the inductor so a real inductor would have inductive, capacitive and resistive parts. This can be modelled and it is possible to obtain the total equivalent capacitance and inductance of the inductor.

Self-resonant frequency of an inductor is defined as the frequency at which, as its name states, the total equivalent capacitance resonates with the equivalent inductance of the inductor. The result is an exceptionally high impedance so the inductors would behave like an open circuit at this frequency. It has to be taken into consideration during the design of an inductor, since the inductor only behaves like an inductor below this frequency [14]. Despite of that, the range of use of transformers does not cover the whole range from 0 GHz to SRF, but that the frequency the transformer stops working properly is lower than the SRF.

The self-resonant frequency is presented in the equation below

$$f_{SR} = \frac{1}{2\pi\sqrt{L_{eq}C_{eq}}} \tag{2.5}$$

where L_{eq} is the equivalent inductance of the inductor and C_{eq} is the total equivalent capacitance of the inductor.

Inductors can be categorized depending on the material and the shape. The typical structure of an inductor is, as it was said above, a wire wound into a coil, sometimes around a core (It can be made of ferrite, iron, air...). Notwithstanding, monolithic inductors are key components in RFICs for wireless communication systems so the document will focus on them [3].

The main undesirable effects and losses related to the monolithic inductors are exposed below:

- **Ohmic losses or resistive losses** depend on the resistance of the material and it transfers the loss into heat. In order to reduce this losses high conductivity materials can be used.
- Since monolithic inductors are build at the top of a substrate, part of the power is transferred to the substrate. **Substrate losses** often decrease the quality factor of the monolithic inductors at high frequencies [4], so it is crucial to reduce this losses during the design. Shielding the substrate with an additional layer between it and the inductor reduces significantly the substrate effect [15] [16].
- **Skin effect**. Probably one of the most important effects when it comes to inductors. While at low frequencies the current through a conductor flows uniformly over the cross section, at high frequencies this current tends to flow in the outer section of the conductor. The effective area of the section is reduced thus the resistance of the conductor increases. This effect makes the resistance of an inductor frequency-dependent as it is shown in section 4 [17].
- At high frequencies, current flows in other undesirable patterns due to the magnetic fields in nearby conductors. This is called **proximity effect** and it has a greater impact than skin effect on the degradation of the quality factor [4].
- Parasitic capacitance between different turns in adjacent layers for spiral inductors.

2.1.1 Transformer

As it was said in the beginning of the chapter, passive components can not generate energy but transform it, hence they are key components in the energy transfer between circuits. A transformer consist of two or more inductive-coupled inductors that provide a power transfer between two circuits when there are not conductive connection between them. Both inductors share the same core for the purpose of achieving an efficient energy transfer. For monolithic transformers, in fact, instead of having two inductors in different legs as it is shown in Figure 2.3, they are often placed on the top of each other in order to reduce the leakage losses, produced by a non-perfect coupling [19].

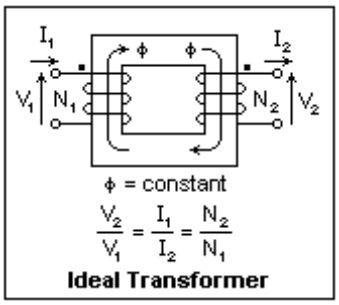

Figure 2.3: Basic two-inductors transformer components

In Figure 2.3, voltages and intensities are defined for a single transformer as well as the number of turns in each. The main equation that reflects the behaviour of the transformer is called the turns ratio of the transformer and can be defined then as

$$n = \frac{V_2}{V_1} = \frac{I_1}{I_2} = \frac{N_2}{N_1} = \sqrt{\frac{Z_2}{Z_1}} \tag{2.6}$$

where N_x refers to the number of turns in port x and Z_x to the impedance on the port x.

Owing to its structure and behaviour, changes in the current intensity or voltage of one circuit change the values in the other. As it was explained in equation 2.1, inductors generate a voltage based on variations of the current intensity. That means inductors work on alternating current (AC) instead of direct current (DC) thus, transformers transmit energy in AC. In some RFICs transformers are used instead of transmission lines because they occupy less area [20]. Main applications of the transformers in RFICs are DC isolation, interstage impedance matching and conversion from single-ended to differential configuration [21].

Since a transformer is formed by two or more inductors, it is affected by the effect and losses related to the inductor such as ohmic losses, skin effect, proximity effect or substrate losses. In addition, transformers suffer losses due to leakage flux and they have capacitive and inductive coupling between the two inductors.

2.2 Transmission line

The current document presents an inductor which fabrication is based on transmission lines' fabrication. Transmission lines offer very low loss and distortion levels, thus they are a key building block for the design of RFICs [22]. Despite there being many different ways to categorize transmission lines depending on shape, length, material, etc., this document will focus on the planar transmission lines such as striplines and microstrip lines. That is because the inductors designed in this document are transmission line-based. The main difference between striplines and microstrip lies in the number of ground planes they have. The structure of a stripline is composed of two parallel ground planes and a plane strip of metal between them, separated from the ground planes by dielectric material. Microstrip is simpler, with only one ground plane separated from the plane strip by the dielectric layer, as shown in Figure 2.4.

There are some properties that can be used to define a transmission line such as its characteristic impedance, attenuation, delay or phase shift. Furthermore, each transmission line has a inductance per unit length and a capacitance per unit length that depends on the material, shape and size of the line. As it will be explained in section 2.3, transmission lines can be modelled by its inductance per unit length and its capacitance per unit length.

In section 2.1 the electromagnetic field of an inductor is described. Since a microstrip can behave like an inductor when one of its ports is grounded, the electric and magnetic field will be similar, with the exception of the presence of a ground plane that changes the electric field significantly as Figure 2.4 shows. Due

to the structure of the microstrip, electric field can be split into two: fringe field and parallel field.

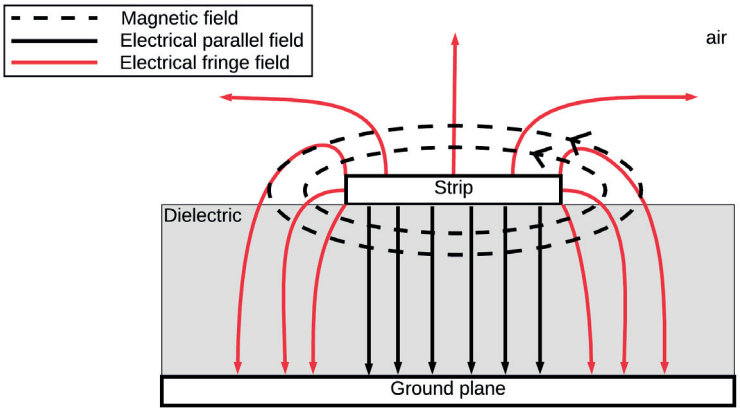

Figure 2.4: Electric and magnetic fields in a Microstrip.

Note that, even though the gap between the strip and the ground is filled with dielectric, part of the electric field is passing through the air. That happens in microstrip lines but not in striplines, where all the electric field is contained within the dielectric material. In striplines then, the capacitance per unit length of the transmission line depends on the dielectric constant of the dielectric material. However, in microstrip lines this capacitance depends on the **effective relative dielectric constant**, that will be somewhere between the dielectric constant of the material and 1(dielectric constant of the air) [17].

Most of the effects and losses that affect microstrip are the same as the monolithic inductors due to the similarities between them [17]:

- **Parasitic capacitances**. The ground plane and the strip form a long capacitance between them, that makes a big influence in the capacitance per unit length mentioned above. As is shown in Figure 2.5 (a), this main capacitance can be split into two: parallel (C_p) and fringing capacitance (C_f). Fringing capacitance and parallel capacitances are created by fringe and parallel fields respectively as Figure 2.4 shows.
- **Resistive loss**. This affects to the attenuation of the signal that is propagating through the transmission line and the phase shift that this signal can suffer.
- **Dielectric loss**. The attenuation is not only caused by the resistive losses but the heating effect on the dielectric material when a signal is propagating, that depends on the dielectric loss factor for the material.
- At high frequencies, **skin effect**, **radiation losses** and **induction losses** can happen and make some influence on the attenuation of the signal as well.

In terms of coupling, inductive and capacitive coupling can affect the microstrip line in the same way as it affects inductors. Figure 2.5 shows how the capacitive

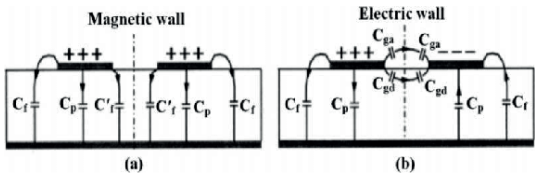

Figure 2.5: Parasitic capacitances in coupled microstrip on a) even mode and b) odd mode (Taken from [23])

coupling affects the capacitance of the line for odd mode while it does not have much effect for the even mode. It is important to consider this in the design of differential devices that usually work on odd mode [18].

2.3 Lumped-element model

In this subsection, models for inductors and transmission lines are exposed.

2.3.1 Transmission line

As it was said in section 2.2, transmission lines are defined by a inductance per unit length and a capacitance per unit length. However, this inductance is not ideal and either the capacitance. Thus, it will be necessary to add a series resistance to the inductor and a parallel conductance for the capacitor in order to modulate the losses through the transmission line, as it is shown in Figure 2.6.

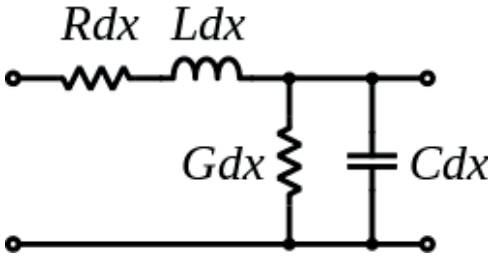

Figure 2.6: Lumped equivalent circuit model of a transmission line.

There is one feature of this model that makes it modular, the line length dependence. Due to that, it is possible to use more than one model in order to achieve a high accurate behaviour, so the transmission line model can be "split" into many sections. The more sections defining the model, the higher the accuracy, but the model will be more complex too. This can be suitable when the transmission line is not homogeneous, for example, when it is bent.

Transmission lines are reciprocal, so the model shown in Figure 2.6 must be changed when a finite number of sections is used. In order to have reciprocal transmission lines its equivalent π-model or T-model should be used instead. Otherwise, a large number of sections is required to approximate the reciprocal device.

2.3.2 Inductor

During the design of an inductor, a compact lumped-element model is often desirable. However, it is necessary to take into account the type of inductor and materials it is made of, so that will change the parasitics and structure of the model. All the references to models in this subsection are related to monolithic inductors.

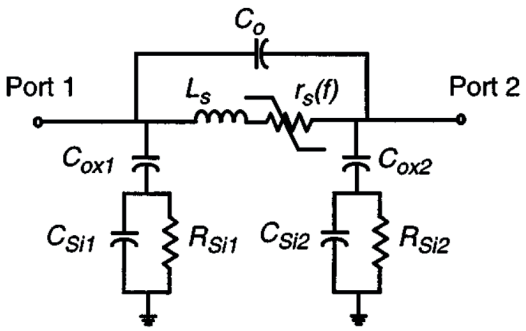

Figure 2.7: Lumped equivalent circuit model of a microstrip inductor [3].

Figure 2.7 shows a simple model for a microstrip inductor, where most of the parasitics are shown. The main part of the design is formed by the series inductance(L_s) and the series resistance($r_s(f)$). The frequency-dependent series resistance is modelling the skin effect, the proximity effect and the ohmic losses of the conductor. In spiral inductors, parasitic capacitances can appear between adjacent turns, this is modelled with the capacitor C_o. C_{ox1} and C_{ox2} refer to the capacitance created between the ground plane of the microstrip and the strip. Finally, substrate effect is modelled with C_{Si1}, C_{Si2}, R_{Si1} and R_{Si2}. Dielectric and induction losses modelling is included in $r_s(f)$, but those losses are normally not significantly in comparison with the ohmic losses.

As it was said in chapter 1, differential inductors are commonly used in RFICs due to its good features. Even though the model described above gives a complete description of an microstrip inductor model, it is necessary to consider the additional effects and parasitics that would be added if the inductor were differential instead of single ended. Often, a central tap has to be considered in differential inductors. This central tap is a new port so the design would have three ports instead of two. Furthermore, the tap is needed to be modelled since it has its own inductance and losses as can be shown in [24] [25] [26]. More complex models can be found in [2], where a multilayer-coplanar-waveguide-based differential inductor is developed or in [22], in which a parasitic inductance is considered.

Q-factor

Although it has been shown above that a complete lumped-element model of an inductor can be quite complex, a very accurate calculation of the quality factor is

rather simple and the model is simplified to an inductor and its equivalent series resistance (ESR). Total impedance and its Q-factor are defined as

$$Z = R_s + jX_s = R_s + j\omega L \tag{2.7}$$

$$Q = \frac{X_s}{R_s} = \frac{L\omega}{R_s} = \frac{2\pi f L}{R_s} \tag{2.8}$$

Where f is the frequency, L is the inductance, Xs is the impedance of the ideal inductance and Rs is the ESR.

2.4 S-parameters

Along this document, some measurements of the electrical parameters are made. Almost every measurement will be based on the scattering parameters so the inductors will be defined as a N-port network [27]. N-port network theory is focused on the electrical characteristics of the ports, so voltage and current will be used to describe them. Several parameters can be extracted from the ports but the basic ones are S-parameters, Z-parameters and Y-parameters. Z-parameters give a measurement of the impedance of the network, and they are calculated when each port, one at a time, is open-circuited. On the other side, Y-parameters calculate the admittance of the network, and they are calculated when each port, one at a time again, is short-circuited.

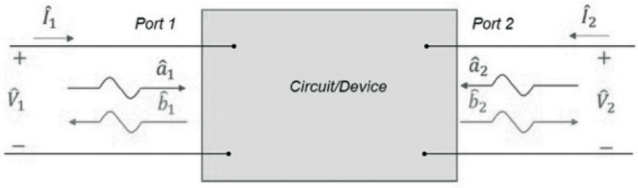

Figure 2.8: Incident and reflected waves in a two-port network (Taken from [28]).

N-port network theory can also describe the ports using incident and reflected waves instead of voltage and current. Figure 2.8 shows a total description of a two-port network, where I_x is the current, V_x is the voltage, $\hat{a}_x$ is the transmitted wave and $\hat{b}_x$ is the reflected wave in port x. The theory of reflection waves is based on the concept of reflection coefficient that can be explained as follows: Every time a transmitted signal arrives at a junction of impedance change the signal splits into reflected signal and transmitted signal. The ratio of the reflected voltage to the incident voltage is called reflection coefficient [17].

S-parameters are obtained then as the ratio between reflected and transmitted wave. The definition of the scattering parameters for a two-port network S-parameters are:

$$s_{11} = \left.\frac{\hat{b}_1}{\hat{a}_1}\right|_{\hat{a}_2=0} \quad s_{12} = \left.\frac{\hat{b}_1}{\hat{a}_2}\right|_{\hat{a}_1=0} \quad s_{21} = \left.\frac{\hat{b}_2}{\hat{a}_1}\right|_{\hat{a}_2=0} \quad s_{22} = \left.\frac{\hat{b}_2}{\hat{a}_2}\right|_{\hat{a}_1=0} \tag{2.9}$$

s_{11} Input port reflection coefficient

s_{12} Reverse gain(isolation)

s_{21} Forward gain

s_{22} Output port reflection coefficient

In terms of displaying the impedance of a transmission line, the Smith Chart is the most suitable tool. All the parameters presented above are based on impedance measuring, so it will be very helpful to display them on the Smith Chart, where both the magnitude and the phase of the parameters can be shown [29]. In this document, a design guide for S-parameters provided by *Keysight Technologies* is followed [30].

2.5 Measurements

In order to characterize the designs of this thesis, some measurements have to be done and different configurations will be used for that. The components will be treated as n-port networks. Single inductors will be defined as a reciprocal 2-port networks, differential inductors as a 3-port networks (central tap is often grounded) and transformers as a 6-port network.

2.5.1 RLGC parameters

The single inductor is based on microstrip so it is possible to obtain the RLCG parameters for the lumped element equivalent circuit (Figure 2.6) as well as other parameters such as characteristic impedance, attenuation, delay or phase shift. The way this parameters are extracted based on Y-parameters and Z-parameters for the 2-port single inductor is shown in the equations below. Note that all the calculations are based on the propagation constant (γ) along the line. This constant measure the changes in phase and magnitude of a signal in a propagation medium.

By theory, The characteristic impedance (Z_0) of a transmission line can be defined as

$$Z_0 = \sqrt{\frac{R + j\omega L}{G + j\omega C}} \tag{2.10}$$

where R, L, G and C refer to the parameters of the lumped equivalent circuit model of a transmission line in Figure 2.6, and Z_0 is the characteristic impedance, that can be calculated from Y and Z-parameters using equation 2.11.

$$Z_0 = \sqrt{\frac{Z_{11}}{Y_{11}}} \tag{2.11}$$

Once the characteristic impedance is calculated, the propagation constant is calculated as well.

$$\gamma_{wrapped} = \frac{1}{l * \text{atanh}(\frac{1}{Z_0 * Y_{11}})} \tag{2.12}$$

$$\alpha = \text{Re}(\gamma_{wrapped}) \tag{2.13}$$

$$\beta_{wrapped} = \text{Im}(\gamma_{wrapped}) \tag{2.14}$$

$$\beta = \text{unwrap}(\beta_{wrapped} * l * 180/\pi, 90) * \pi/180/l \tag{2.15}$$

$$\gamma = \alpha + j\beta \tag{2.16}$$

where γ is the propagation constant, α is the attenuation constant in $Neper/m$, β is the phase constant in rad/m and l is the total length of the transmission line. Equation 2.17 shows the angular frequency that, with γ and Z_0, are used to calculate the RLGC parameters in equations 2.18 and 2.19. Note that those parameters are expressed in function of the length, so the units would be H/m for the inductance, F/m for the capacitance, S/m for the conductance and Ω/m for the resistance.

$$\omega = 2\pi f \tag{2.17}$$

$$R_s = \text{Re}(\gamma Z_0) \qquad L_s = \frac{\text{Im}(\gamma Z_0)}{\omega} \tag{2.18}$$

$$G = \text{Re}(\gamma / Z_0) \qquad C_p = \frac{\text{Im}(\gamma / Z_0)}{\omega} \tag{2.19}$$

The attenuation, effective relative dielectric constant and phase shift can be calculated as well with the following equations

$$\alpha_{dB} = 20\alpha log(e) \tag{2.20}$$

$$v = \omega/\beta \tag{2.21}$$

$$\varepsilon_{eff} = \sqrt{\frac{c_0}{v}} \tag{2.22}$$

$$\phi = \beta * 180/\pi \tag{2.23}$$

where α_{dB} is the attenuation expressed in dB/m, v is the propagation velocity in m/s, ε_{eff} is dimensionless and ϕ is the phase shift expressed in degrees/m. These parameters can define the characteristic of a transmission line and, in this case, a transmission line-based inductor.

2.5.2 Inductance, resistance and Q-factor

In the design of an inductor, the three main parameters of interest are the inductance, the resistance and the quality factor. Those are calculated based on Y and Z-parameters. As it was said in section 2.4, Y-parameters are calculated for a port when the rest of the ports are shorted, and Z-parameters when the rest of the ports are open. It is also important to make a difference between the inductance and resistance per length of the lumped equivalent circuit calculated in equation 2.18 (R_s and L_s) and the effective inductance or resistance of the inductor seen from the port. The quality factor will be the ratio between the inductance and the resistance, and two configurations are possible: single-ended and differential, both shown in Figure 2.9.

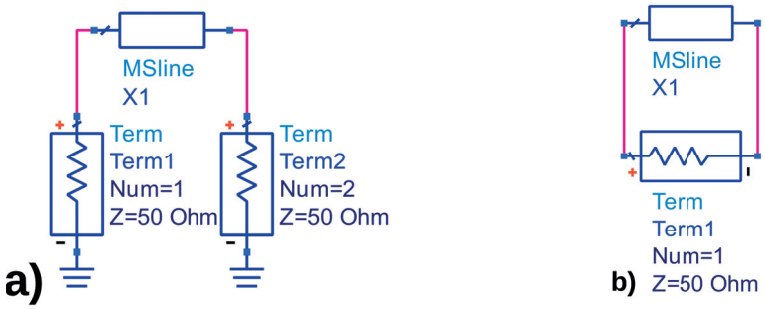

Figure 2.9: a) Single and b) differential port configuration for a single inductor

However, it is possible to calculate the differential response with a single-ended port configuration, so this will be the chosen one. The single-ended parameters can then be calculated with the following equations [25]:

$$L_{se} = \frac{\mathrm{Im}(1/Y_{11})}{\omega} \qquad R_{se} = \mathrm{Re}(1/Y_{11}) \tag{2.24}$$

$$Q_{se} = \frac{\mathrm{Im}(1/Y_{11})}{\mathrm{Re}(1/Y_{11})} = \frac{\omega L_{se}}{R_{se}} \tag{2.25}$$

On the other hand, it is necessary an impedance transformation to obtain differential parameters, as can be shown in equation 2.26.

$$Zd = Z_{11} + Z_{22} - Z_{21} - Z_{12} \tag{2.26}$$

and parameters are calculated in the same way as the single-ended ones [51]:

$$L_{diff} = \frac{\mathrm{Im}(Zd)}{\omega} \qquad R_{diff} = \mathrm{Re}(Zd) \tag{2.27}$$

$$Q_{diff} = \frac{\mathrm{Im}(Zd)}{\mathrm{Re}(Zd)} = \frac{\omega L_{diff}}{R_{diff}} \tag{2.28}$$

These six parameters along with S-parameters will be used in order to adjust the lumped-element equivalent models presented on the next section. The single-port configuration for the differential inductor is presented in Figure 2.10, a). Due to the fact that differential inductors are mainly used in applications where the central tap is biased or shorted, port 3 (central tap) is shorted for this calculus.

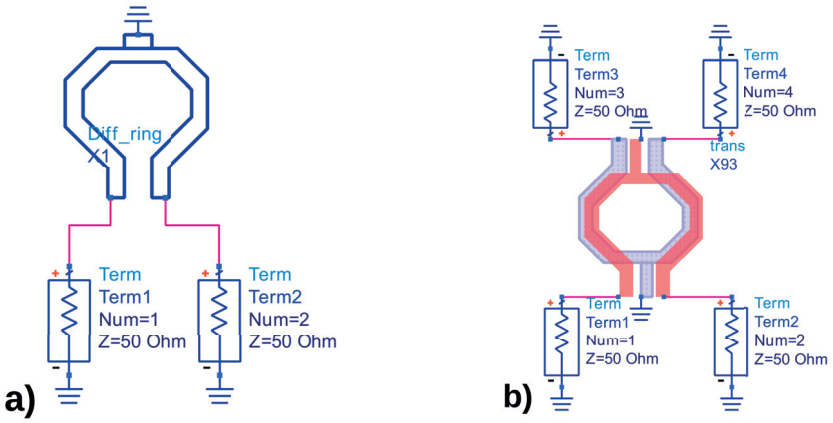

Figure 2.10: Single port configuration for a a) differential inductor and b) transformer

In the case of the transformer, the six parameters $(L_{se}, R_{se}, Q_{se}, L_{diff}, R_{diff}, Q_{diff})$ calculated before give some information about the circuit, however, the complexity of the 6-port network makes necessary to take different measurements with different configurations depending on the purpose of the transformer.

2.5.3 Transformer measurements

A measure of the inductance and the Q-factor of the transformer's windings is usually necessary to characterize it [33]. Although several configurations can be used to test the transformer, the most typical way to define the self-inductance is the single-ended to single-ended configuration without bias, as shown in [20] and [31]. As explained in previous chapters, Y-parameters will imply to have a shorted output, so Z-parameters are used instead. Self-inductance and Q-factor of the transformer shown in the results chapter are calculated with the following equations:

$$L_p = \frac{\mathrm{Im}(Z_{11})}{\omega}, L_s = \frac{\mathrm{Im}(Z_{22})}{\omega} \tag{2.29}$$

$$Q_p = \frac{\mathrm{Im}(Z_{11})}{\mathrm{Re}(Z_{11})}, Q_s = \frac{\mathrm{Im}(Z_{22})}{\mathrm{Re}(Z_{22})} \tag{2.30}$$

where L_p and L_s corresponds to the self-inductance in the primary and the secondary winding respectively and Q_p and Q_s the Q-factor for the primary and

the secondary [20]. Although the inductance and Q-factor of the windings give some useful information, it is necessary to measure the gain (S_{12} or S_{21}) to fully characterize the energy transfer in the transformer. As it was explained above in section 2.4, every time a signal arrives a junction of impedance change, part of the signal reflects, resulting in loss of energy. That happens in the ports of the transformers, where, if the port is not matched correctly, part of the energy is reflected. Based on that, it is possible to define the **maximum available gain** as the maximum gain of the transformer if all the ports where perfectly matched. If a mismatch happens, a matching circuit can be added in order to achieve (or at least get close to it) this maximum gain.

In transformers, there are two ways to define the coupling. First and well-known way is to separate the coupling into inductive and capacitive. This separation is of interest in the description of the transformer model in following sections. Another way to express the coupling in a transformer are the mutual coupling factors. The coupling can be divided then in two: a mutual reactive coupling factor (k_{Im}) and a mutual resistive coupling factor (k_{Re}), both calculated with equation 2.31 [32] [34]. In this way, those coefficient separate the coupling in reactive and resistive instead of inductive and capacitive.

$$k_{Im} = \sqrt{\frac{\mathrm{Im}(Z_{12})\mathrm{Im}(Z_{21})}{\mathrm{Im}(Z_{11})\mathrm{Im}(Z_{22})}}, k_{Re} = \sqrt{\frac{\mathrm{Re}(Z_{12})\mathrm{Re}(Z_{21})}{\mathrm{Re}(Z_{11})\mathrm{Re}(Z_{22})}} \tag{2.31}$$

Another characteristic of the transformers can be defined as amplitude and phase unbalance. By definition, a balanced two-terminal impedance has neither of its terminals connected to ground, while an unbalanced impedance has one of its terminals grounded [35]. Balanced-to-unbalanced mode conversion is one of the applications of the transformer, so it is necessary to give a measure of the "symmetry" of the device. For that, an amplitude is applied to the primary and the two resulted voltages are compared in order to obtain the difference in amplitude and phase with respect each other, as shown in Figure 2.11.

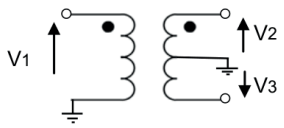

Figure 2.11: Unbalance in transformer (Taken from [35]).

In this test bench, the two output voltages are in anti-phase, so the difference in phase should be 180°. Any deviation from this value is measured as the phase unbalance, as it is explained in [35]. The difference in amplitude and phase can be calculated with the equations below.

$$\texttt{amplitude unbalance}(dB) = 20log_{10}(\frac{|V_2|}{|V_3|}) \tag{2.32}$$

$$\texttt{phase unbalance}(deg) = \text{phase}(V_3) - \text{phase}(V_2) - 180 \tag{2.33}$$

All this measurements presented in this chapter are used to get all the results presented in section 4.

Chapter 3
Method

A description of the steps made along the thesis can be shown in this chapter. First, an overview of the software and technology used for this thesis is presented. After that, the physical description of the microstrip inductor designs is shown. The final part will be divided in the simulation setting, where the parameters for the simulations are set, the characterization part, where measuring of the inductors are made, and the modelling part, where the lumped-elements models for the inductor are designed.

3.1 Software and technology

As indicated in Chapter 1, the software used for this thesis is ADS, an electronic design automation software for RF, microwave and high-speed digital applications that supports both layout and schematic design [36]. The design of the inductors in this thesis are described at layout level, and electromagnetic simulations will be the most important feature of ADS that will be used. In terms of electromagnetic simulations, ADS has three main solutions:

- *Momentum Microwave*. Momentum μW computes S-parameters for general planar circuits, such as microstrip, stripline or coplanar waveguide [37].
- *Momentum RF*. While Momentum μW uses full-wave formulation, Momentum RF uses quasi-static formulation [38]. The purpose of this simplification is to have more efficient simulations for RF. That means Momentum RF is suitable for circuits that are electrically small, geometrically complex and it do not radiate [38].
- *Finite Element Method*(FEM). Although Momentum can simulate multilayer structures, FEM provide the best solution for random-shaped passive three-dimensional structures [39]. FEM simulations often manage a lot of data so it usually takes more time than Momentum simulations.

Even though all the structures described in the document are electrically small [38], the substrate used is electrically large above 7.52 GHz and a warning pops up if a Momentum RF simulation is run, so it is not suitable for this thesis. On the other hand, FEM simulations implies a high complexity of the mesh so

the simulation time will increase drastically. As a result of these considerations, electromagnetic simulations will be carried out by Momentum μW along this thesis.

The designs of this work are are based on microstrip transmission lines above a ground plane, raised from the semiconductor. The choice of microstrip instead of stripline or coplanar waveguides is explained as follows:

- The raised ground plane in microstrip lines provides isolation from the substrate so it reduces losses and parasitics. Coplanar waveguides have not raised ground plane so they are exposed to this undesirables effects from the substrate.
- The design of this inductor is later extended to the design of a transformer, that consist of two inductors placed on the top of each other. Striplines have a top ground plane that does not allow this.

Every design of this thesis is built over the custom-made technology described in the Nanoelectronics Student Component Library of Lund University [9]. The multilayer stack defined by the technology shows several dielectric and conductor layers, as well as vias to interconnect them, as shown in Figure 3.1.

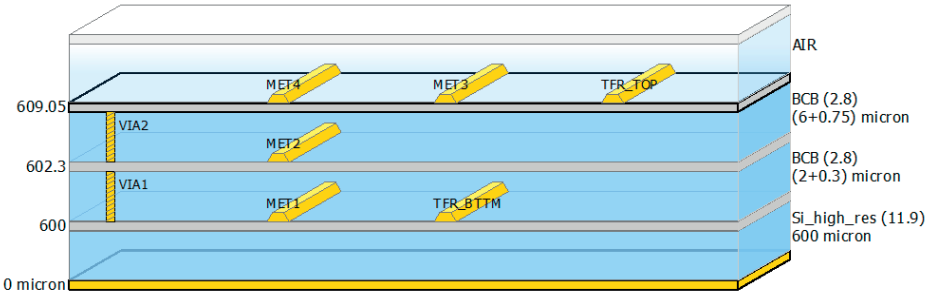

Figure 3.1: Multilayer stack of the custom-made technology used in this thesis.

Most of conductor layers and vias in the figure above are made of gold, except for TFR_TOP and TFR_BTT, which are made of nickel-chrome. At the bottom is placed the silicon substrate and benzocyclobutene (BCB) is used as an interlayer dielectric.

As it was shown in Figure 2.4, a microstrip is composed of a strip, the ground plane and a dielectric layer between them. The microstrip inductor will be in MET3 (thickness 0.75 μm) and the raised ground plane will be in MET2 (thickness 0.75 μm). The dielectric layer between them is a 6μm-thick BCB layer.

For the transformer, it will be necessary to replace the air layer of Figure 3.1 with a 2μm-thick BCB layer. A new gold conductor layer (MET5) on the top of this new dielectric layer will be added, with the same thickness as MET2 and MET3, as well as a new 0.5μm-wide via (VIA3), that connects MET3 with MET5.

The high conductivity of the gold used for the strips will reduce the ohmic losses that depends on the resistance of the line. With regard to the dielectric layer, some characteristics of the BCB make it suitable for mm-wave microstrip, such as low losses and permittivity over a wide frequency range [40]. Also, it has

been proved that a thick BCB layer reduces substrate losses working over a silicon substrate [41].

3.2 Inductor Designs

Nowadays, performance and cost of high-speed circuits is becoming highly influenced by the interconnections. Therefore, layout solutions are acquiring more importance for integrated circuits (IC) design [42]. Several sizes an shapes are used in regard to monolithic inductors. One suitable option in the design of monolithic inductors are planar transmission lines, that behaves like an inductor when one of its ports is grounded, such as microstrip or stripline. Every structure described in this document is microstrip-based.

The design follows a bottom-to-top structure, the simplest structure is designed first and more complex structures based on the previous ones are created afterwards. In section 2.3 the lumped equivalent circuit of a transmission line is presented, which is mainly composed of a capacitive part and an inductive part. Due to its characteristics, a narrow microstrip would behave more like an inductor, while wide microstrip behavioural would be more similar to that of a capacitor. The characteristic impedance of a transmission line is defined by the width of the line. In the technology used in this thesis, approximately $8\mu m$ of width in MET3 ($0.75\mu m$ thickness) implies around 75Ω, while a double width would form a 50Ω transmission line.

In this work, the base inductor will be a 75Ω transmission line, shown in Figure 3.2, a), from which some modifications will be made. A $100\mu m$ long 75Ω transmission line will have an inductance of approximately 35-40 pH, which value is suitable to work on a resonator of a VCO like the one shown in [43]. Note that P2 is assumed grounded through the use of Y-parameters and P3 is always grounded (Figure 3.2). The description of a single inductor allows to build more complex structures based on it.

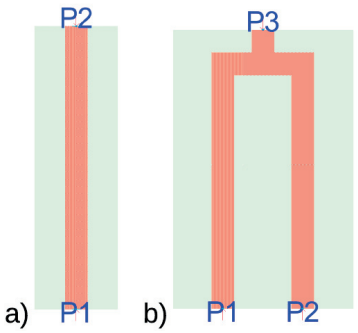

Figure 3.2: a) Microstrip line and b) differential inductor with 2F structure. Ports expressed as Px, ground plane in green(MET2) and the strip in red(MET3).

Even though the design of single inductors is essential, differential configurations have become the dominant choice in RFICs. Hence, a differential inductor design

is needed [44]. The first differential structure consists of two parallel lines joined by the centre tap as shown in Figure 3.2, b). The total length of this differential inductor will be $200\mu m$. For a differential inductor, this structure may seem simple, nonetheless, similar structures give good performance in VCOs as it is shown in [15] and [16].

The sharp 90-degree corners of the inductor presented in Figure 3.2, b) may cause undesirable effects such as radiation, losses or coupling, therefore, layout designers try to avoid sharp corners. The ring structure presented in Figure 3.3, a) reduces, not only the undesirable effects of sharp corners, but the coupling between the two branches as well. The balance between performance and simplicity that is offered by this ring structure makes it suitable for high-Q monolithic differential inductors [45].

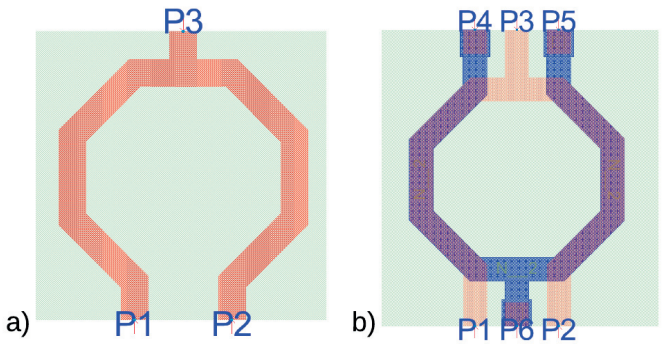

Figure 3.3: a) Differential inductor with Ring structure and b) transformer based on ring structure. Ports expressed as Px, ground plane in green(MET2), first winding in red(MET3) and second winding in blue(MET5).

At the top of the design, a transformer based on the ring structure is developed. A new ring differential inductor(MET5) is placed at the top of the inductor of Figure 3.3, a) (MET3), both completely overlapped in Figure 3.3, b). MET5 and MET3 are connected through VIA3.

Based on the 75Ω line, several transmission lines are designed with the purpose of looking at the behaviour of them when some parameters are changed such as length or width. Lengths for all the designs of this thesis are shown in Appendix A (table A.1). Different variations on the length of the inductors occurs due to design decisions.

3.3 Simulation Setup

An exhaustive choice in the simulation settings is necessary to obtain reliable data from the simulations. Mesh settings, ground plane extension and port configuration will be taken into account along this section. The single microstrip inductor shown in Figure 3.2, a) will be used for the simulations of this section.

3.3.1 Port setting

The pin selection and port definition in ADS is crucial since it will define the S-parameters obtained in the simulations. Depending on the shape of the zone excited by the pin in the layout, pins can be defined in 3 types: point pin, edge pin and area pin.

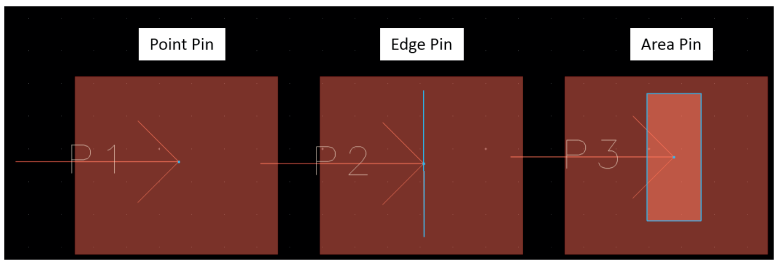

Figure 3.4: Pin types (taken from [46])

All pin types mentioned above are supported by Momentum. Pins are placed in the layout and the way they associate with each other defines the port configuration. Edge pins are used along this work. Ports are defined by two terminals, a positive and a negative, that can be pins or ground planes.

Differential inductors are usually used, as its name suggests, in differential mode, indeed, RFICs are often designed to work in differential configuration [44]. That means the signals in the two branches of the inductor are in anti-phase so the inductor is working on odd mode. As it can be seen in Figure 2.5, the coupling of the inductor is different depending on the mode the inductors are working on, so it is important to have several measurements of the inductor to model it properly.

Regarding the excitation of a two-terminal circuit, two main configurations are possible: differential and single-ended. For differential measurement one port that excites the two pins in anti-phase is enough. On the other hand, two ports are needed for the single-ended port configuration. In this thesis, two-port configuration will be used. This configuration is usually more flexible, since it is possible to convert the two-port single-ended data into differential data so there is not need to run two simulations [47]. The conversion basically converts the single-ended impedance into differential impedance and it will be shown in section 2.5.

3.3.2 Ground plane extension

The ground plane makes an influence in the inductor, so the dimensions of the raised ground plane have to be taken into consideration. It is called ground extension to the distance between the transmission line edge and the ground edge in the X-axis, as shown in Figure 3.5. If ground extension is too small then fringing field shown in Figure 2.4 is limited and the total capacitance of the line will decrease.

For this reason, it is necessary to extend the ground plane until the effect of it is the same as an infinite ground. Several values have been tried and it is possible to see saturation in the parameters, for example, in the characteristic impedance shown in Figure 3.5. All the different parameters that define the transmission line

follow the same behaviour in terms of saturation. Since simulation time does not increase significantly when ground extension increases, so the value used in this document will be 100 μm.

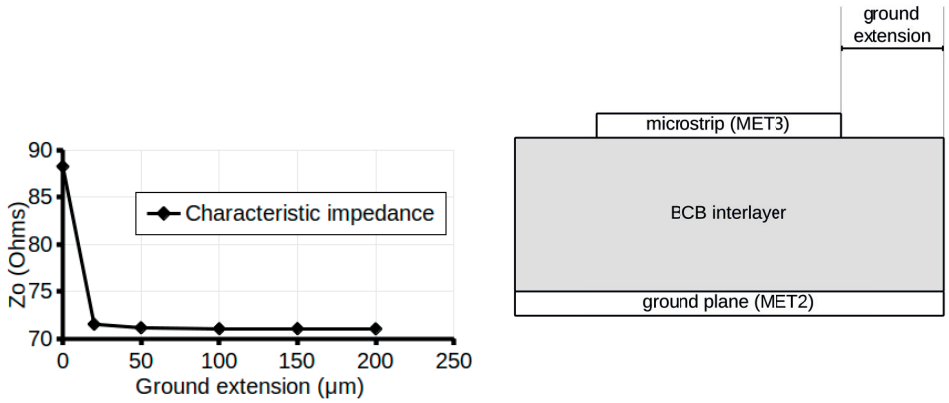

Figure 3.5: Characteristic impedance function of the ground extension (left) and section of the microstrip line where the ground extension is shown (right)

3.3.3 Mesh setting

The mesh is a geometric-based pattern that divides the circuit in cells. The larger the number of cells in a circuit, the more accurate the circuit is. Increasing the number of cells implies more complexity so simulation time will increase too [48]. The choice of the characteristics of the mesh decides the reliability of the simulations done so it is important to carry out a study of the values of the mesh that gives us good results without consuming too much time. Mesh settings can be global or can be assigned to a specific part of the circuit, but in this work only global settings will be used. Three main parameters decide the accuracy of the mesh: mesh density (cells/wavelength), edge mesh (edge width) and transmission line mesh (number of cells in width) [48].

- *Mesh density* is related to the circuit length measured in wavelengths and the number of cells along the length of the circuit or component. In the case of this thesis, it will define the cells on the long direction of the transmission line. Mesh density depends on the mesh frequency, that in this case will be selected as the highest simulation frequency(200 GHz).
- *Transmission line mesh* refers to the number of cells along the width of a geometry. This is often useful for the designs where straight geometry is used, such a transmission lines.
- *Edge mesh* is used to increase the accuracy next to the edge of the structure. It is defined as the distance between the edge and the first line that defines a cell. It can be useful to notice how the current intensity, and therefore, the inductance increases when it comes to the outer section

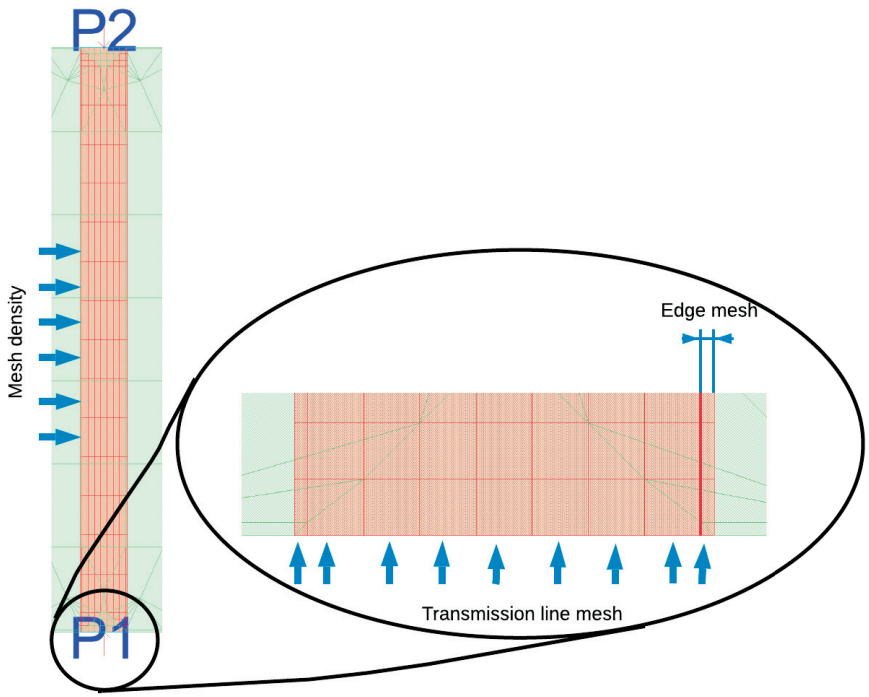

Figure 3.6: Mesh parameters for a microstrip. Mesh density = 100 cells/wavelength, 9 cells in width and 0.25μm edge mesh. Ports expressed as Px, ground plane in green(MET2) and the strip in red(MET3).

Figure 3.6 shows the result of the mesh setup study carried out along this section, where mesh density defines the partitions along the line length. To identify the transmission line mesh and the edge mesh, a zoom to the line is desirable. As explained above, the number of cells per width corresponds to the number of partitions along the line width, as it is shown in the inset of Figure 3.6.

The values that will be checked in this section are the following: Characteristic impedance, attenuation, phase shift, delay, effective relative dielectric constant and the RLGC parameters of the lumped equivalent circuit shown in Figure 2.6, and its calculation is derived in section 2.5. A flux diagram of the steps in this thesis is shown in Appendix A (Figure A.1).

In the beginning, edge mesh will remain automatic, so mesh density and transmission line mesh have to be set. First, transmission line mesh is not selected and edge mesh is set in auto. The mesh will then have 3 cells per width since it is the minimum number of cells in width when edge mesh is set [48]. With those values it is possible to see a saturation around 100 cells/wavelength for the mesh density. Note that this value of the mesh density is based on not trustworthy values for the transmission line mesh, so, after fixing the transmission line mesh parameter, it will be necessary to check the mesh density again. After that, a sweep for the transmission line mesh is done where odd values from 3 to 11 are taken. Because of the skin effect and the fringing field, it will be less information

in the centre of the section of the microstrip than near the edges, that is why an odd number of cells will be selected.

Figure 3.7 shows how inductance and the characteristic impedance changes with the sweep and it is possible to see some saturation between 7 and 9 cells per width. Note that, even though only inductance and characteristic impedance are shown here, several values has been taken into account.

Considering all the parameters calculated, less than 0.05% of relative error is obtained between 9 and 11 cells per width in the worst case (inductance). Simulation time evolution can be shown in table 3.1, where it can be seen that the maximum difference happens between 9 and 11 cells per width.

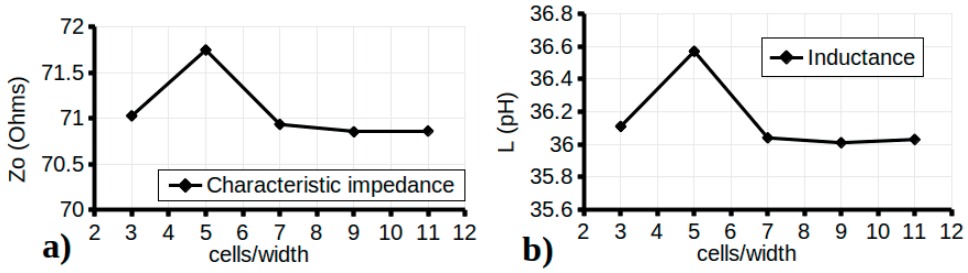

Figure 3.7: a) Characteristic impedance and b) inductance (mesh density=100 cells/wavelength)

Cells per width	3	5	7	9	11
Simulation time	01:15	01:10	01:20	01:30	01:50

Table 3.1: Simulation time for mesh density = 100 cells/wavelength and automatic edge mesh

For the edge mesh adjust, a mesh density of 100 cells/wavelength and 9 cells per width are used. Edge mesh selection is motivated by the two main effects that affect a microstrip in the distribution of the current along the strip: skin effect and fringe fields.

Monolithic inductors can have their Q-factor affected by the skin effect because it makes the resistance and the inductance frequency-dependent [4]. Along this thesis, this effect can be noticed in two different ways:

- As said in section 2, skin effect produces a variation on the resistance with the frequency. This variation of the resistance with the frequency is almost linear for high frequencies [49]. In section 4, RLGC parameters are calculated for a single microstrip inductor and this variation with the frequency can be easily seen.
- Its definition says that what provokes this effect is that intensity tends to flow in the outer section of the line. Taking then different points of the microstrip measuring it then will give us the variation of the intensity, thus, the inductance in relation with its proximity to the edge. This relation

should be exponential so the closest it gets to the edge, the higher intensity through it [49].

Moreover, the fringe field shown in Figure 2.4 contributes to increase the current through the edges of the line as well. This effects affect the current distribution in some way that losses increases when they are approaching the edge, until they reach a maximum and start to decrease. This shape can be seen in Figure 3.8, a).

In order to consider those effects in the models, a proper edge mesh should be selected. Different measurements from $0.05\mu m$ to $0.85\mu m$ are taken and the variation of the attenuation and the inductance of the inductors is shown in Figure 3.8.

For a gold microstrip as the one used along this document, the skin depth is around $0.25\mu m$ at 100 GHz as can be calculated with the equation 3.1 [50].

$$\delta = \sqrt{\frac{2}{\omega\mu\sigma}} \tag{3.1}$$

Where δ is the skin depth, ω is the angular frequency, μ is the permeability and σ is the conductivity of the material.

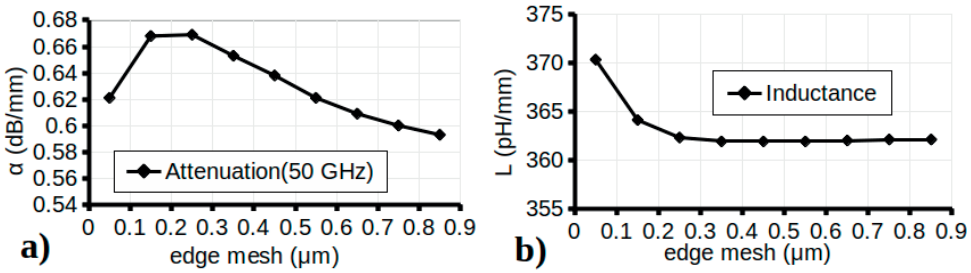

Figure 3.8: a) Attenuation and b) inductance of a microstrip for different edge mesh

As Figure 3.8 presents, the graph for the inductance is exponential, as expected, while the attenuation shows the behaviour explained above. With the purpose of not underestimate the losses of the line, the skin depth value is taken [50]. Note that this measurement refers to the maximum attenuation point. The final configuration for the thesis then is mesh density = 100 cells/wavelength, transmission line mesh = 9 cells/width and edge mesh = 0.25 μm. In order to check the accuracy of the selected meshing setup, a comparison with a very complex mesh is shown in the Figure A.2 of the Appendix A.

3.4 Measurements

The first step to follow after drawing the layout of the inductor is running an electromagnetic (EM) simulation using Momentum μW. The result of this simulation could be used to create an EMmodel that characterizes the inductor component

that will be used for the simulations. After that, it is possible to place those components on a schematic to measure the mentioned parameters in section 2.5.

The measurements are divided into the extraction of the RLGC parameters of the line and the characterization of the inductors through a measurement of the inductance, resistance and quality factor. RLGC parameters extraction will be useful in the definition of the model, while the measure of the inductance and resistance will help to define the behaviour of the component as well as verification of the model.

Apart from the measurements of inductance and resistance, some extra measurements are taken for the transformers, such as impedance gain, unbalance amplitude and phase or frequency range. Depending on the purpose of the component, different measurements have to be done. Since this thesis structure follows a general research, several configurations are considered and comparison of different kind of inductors are tested.

3.5 Modelling

Owing to the critical role of inductors and transformers in RFICs, a performance optimization is needed. For that, it is necessary to define not only the characteristics that describe the inductor, but an equivalent circuit that models the effect of the parasitics, specially at high frequencies [22]. In this section, a description of the models used in this thesis is done. In the same way the design of the inductors follows a bottom-to-top structure, each model will be based on the previous one, growing in complexity as it does so.

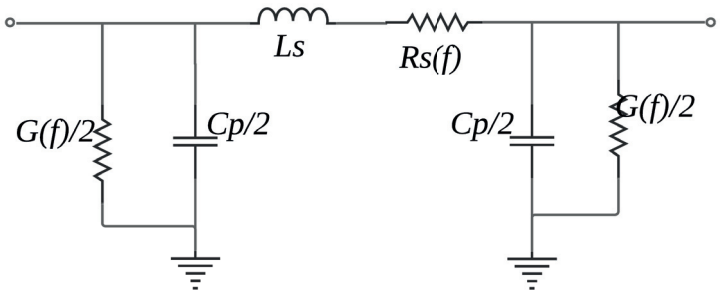

Figure 3.9: Section of the lumped equivalent circuit model of a microstrip inductor for this thesis

Following this structure, the first model to take into consideration will be the single microstrip inductor model. The lumped equivalent circuit of a microstrip inductor is shown in Figure 2.7. Due to the technology used, the raised ground plane of the microstrip blocks the substrate effect so the parasitics related to that will not appear. Furthermore, the current structure only has one turn so there is not capacitive coupling between adjacent turns of the inductor. Considering that capacitors are not ideal, a conductance should be placed in parallel with the capacitance between the strip and the ground plane. The resulting model turn

out to be a π-model version (the inductor is reciprocal) of the equivalent circuit for a transmission line shown in Figure 2.6. Despite the fact that it is possible to use both a π-model and a T-model for a reciprocal transmission line, π model is generally recommended in modeling, due to the creation of a new node in a T representation [52]. The circuit model used for the inductor is shown in Figure 3.9 where R_s, L_s, C_p and G are the RLGC parameters calculated (at 100GHz, since this is the frequency of interest) following the formulas of section 2.5.

Two facts are necessary to take into account: First, all those parameters are dependent on the microstrip line length, so the transmission line can be represented with a multi-component model in which each section describes only a small section of the line. Four sections are selected for the single inductor because it gives a good accuracy and relatively low design complexity.

Second, R_s has a linear dependence with frequency, and as it will be seen in chapter 4, G has a linear dependence with frequency too. In terms of the dependence with the frequency, the expression for the resistance and the conductance will be

$$R_s(f) = R_{DC} + R_s * x * f \tag{3.2}$$

$$G(f) = G_{DC} + G * y * f \tag{3.3}$$

where R_s and G are the parameters calculated above at 100GHz, R_{DC} and G_{DC} are the resistance and the conductance of the inductor at 0Hz and x and y define the slopes of the linear dependence with frequency for resistance and conductance respectively. The DC parameters values, as well as the slopes, are calculated from the graphs of the resistance and the conductance that can be obtained with formulas 2.18 and 2.19. Those graphs are almost linear around the band of interest (W-band), but the behaviour out of this band may differ. Therefore, those parameters may be changed to fit the model.

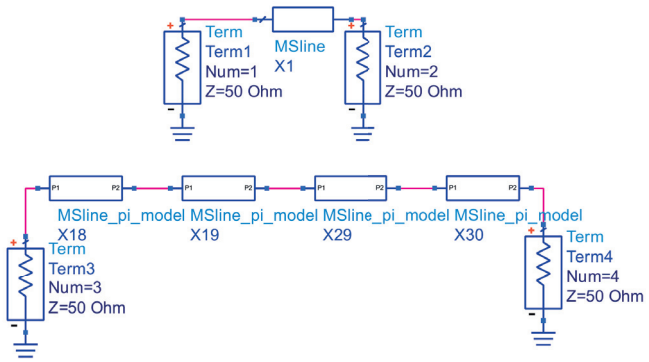

Figure 3.10: Model of a microstrip single inductor (down) and single inductor (up) for N = 4 stages

Figure 3.10 shows the 4 sections in which is divided the model of the microstrip inductor. In the detailed section of the model shown in Figure 3.11 it is possible to

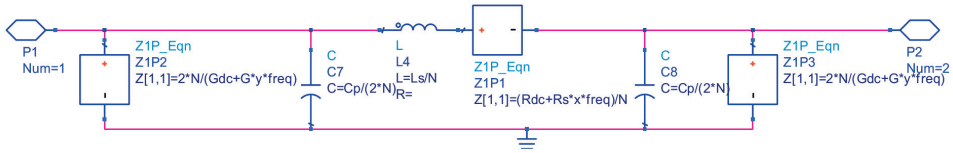

Figure 3.11: π-configuration of a section of the model of a transmission line stub

see how the component *Z1P_Eqn* is used instead of a simple resistor to achieve the dependence with frequency.

What comes next in the list is the differential inductor modelling and two different structures have to be taken into consideration: 2 fingers structure (Figure 3.2, b)) and ring structure (Figure 3.3, a)). Prior to that, a coupling study is needed so both capacitive and inductive coupling can be modelled properly.

Coupling study

Two single microstrip are placed in parallel separated by a variable distance. 10, 20, 30, 40 and 50μm will be the set of values for this gap. The objective of this study is to get the relation between the coupling and the gap length with the purpose of applying this coupling to the model of the differential inductor and the transformer.

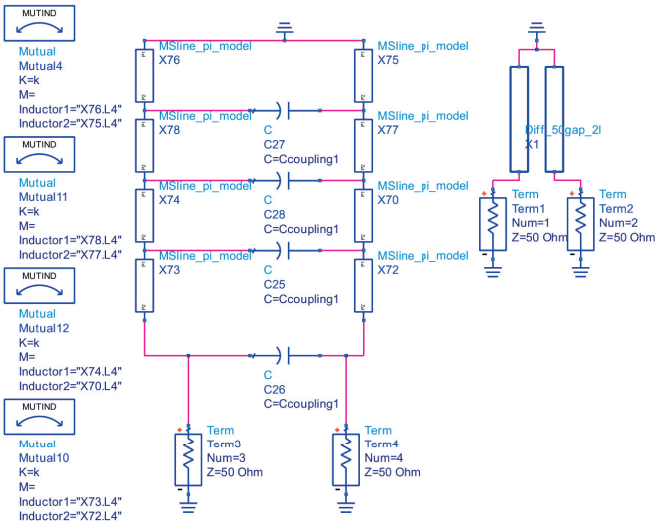

Figure 3.12: Schematic test bench for the coupling study

To get the coupling between them, two single inductor models are placed as shown in Figure 3.12 and capacitors between the two branches emulate the capacitive coupling. MUTIND ADS component is used for the inductive coupling, that indicates the mutual inductance between the sections of the model, and the

coupling coefficient will be used to model that (mutual inductance can also be used instead of the coupling coefficient [53]).

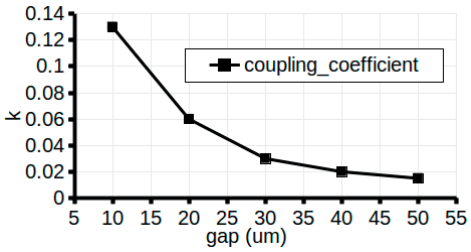

Figure 3.13: Inductive coupling coefficient between the two lines

As a result of this study, it is easy to notice that capacitive coupling does not make a big influence so we can conclude that capacitive coupling is negligible. However, there is an inductive coupling between the branches and it increases exponentially when the gap decreases, as can be seen in Figure 3.13.

The simplest differential structure proves to be the 2 fingers (2F), since it only consists of two parallel straight lines separated by $20\mu m$ that are joined by the central tap. Four $21.5\mu m$ sections will be used in each branch for the straight part, and an additional section with $14\mu m$ for the horizontal part next to the central tap, which is modelled with a $11\mu m$ section as it is shown in Figure 3.14.

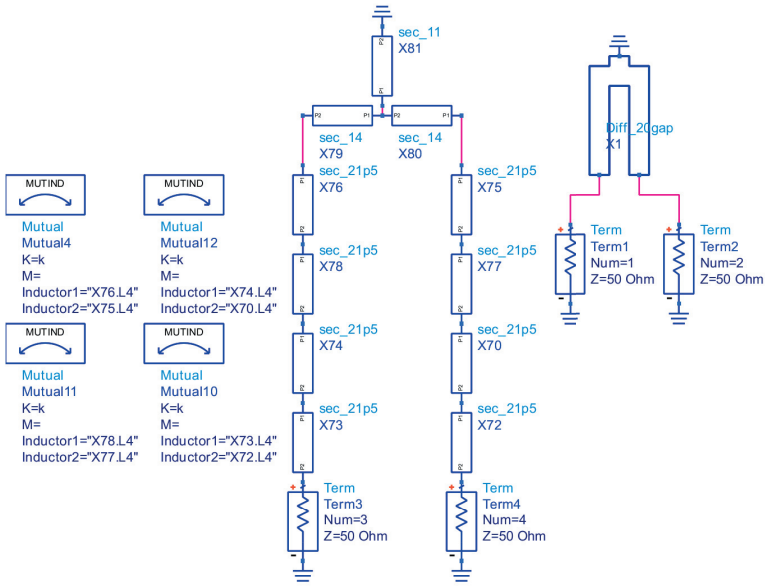

Figure 3.14: Test bench for the 2 fingers differential inductor

Note that the inductive coupling is not desirable in this case, so in order to dim this coupling, a ring structure shown in Figure 3.3, a) is used [45]. Note that 3

different coupling coefficients are considered in the ring structure but only $k3$ has a non-negligible value, so the value for that coefficient only refers to the inductive coupling between the two 11 μm segments close to the ports.

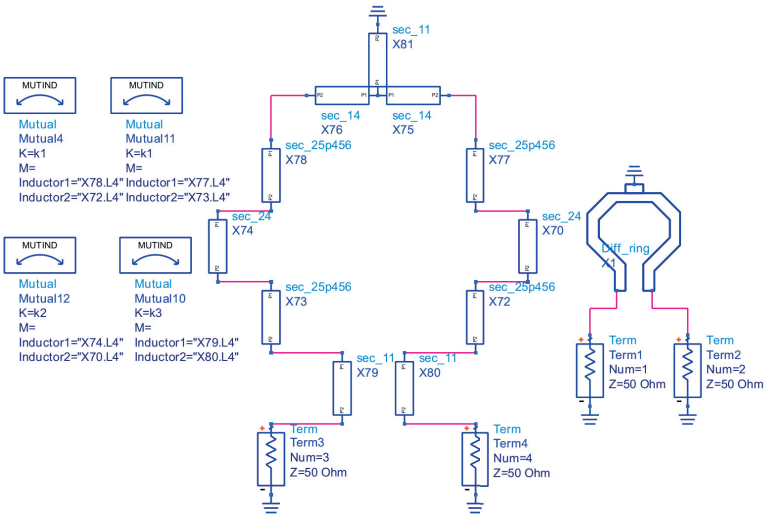

Figure 3.15: Test bench for the ring differential inductor

Despite the fact that the model for a single inductor shown in Figure 3.10 is divided into four equal sections, this division does not have to be in equal parts. Model presented in Figure 3.11 can be modelled depending on the length of the section, that is useful in non-homogeneous lines such as the differential inductors of this thesis. For this modelling, the selection of the N parameter is done internally and it is computed with the equation 3.4.

$$N = \frac{L_{total}}{L_{segment}} \tag{3.4}$$

where L_{total} refers to the length of the line used to obtain the RLGC parameters, 100 μm in this thesis, and $L_{segment}$ is the length of the segment we are modelling. The notation for those component is sec_x, where x is the length of the segment.

Several effects have to be considered regarding differential structures. The first consideration is that, even though the length of one branch is the same as the length of the single inductor modelled before, the central tap adds an extra length to the design. On the other hand, the presence of corners reduces the electrical path of the current so the electrical length is reduced. Corners are often translated into an increase of the losses, since energy can be lost there too.

As indicated in section 3.3.2, an extension in the ground was made for the purpose of having an "infinite ground" at both sides of the inductor so the fringe field does not get lost. In the differential inductor structures, nonetheless, the superior edge of the horizontal 14μm sections are only 8 microns away from the edge of the ground, so part of the fringe field is limited at this point.

Following the bottom-to-top structure mentioned above, the model for the **transformer** will be based on the model of the ring differential inductor as it was presented in Figure 3.3, b). A ring model such as the one shown in Figure 3.15 for each winding will be considered and additional inductive and capacitive coupling will be added between them. Both types of coupling will be added separately for each section of the wing, linking each section with the one that is just above/below.

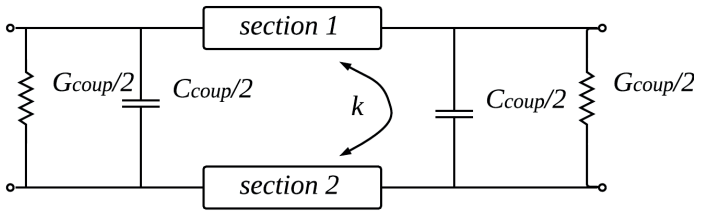

Figure 3.16: Coupling between two sections.

This way of modelling a transformer is quite common for monolithic inductors in RFICs, as can be seen in [54] and [55]. The used structure is shown in the Figure 3.16 where the sections are described in Figure 3.9, section 1 and 2 corresponds to the primary and secondary winding sections and k represents the inductive coupling between their respective L_s components. The capacitive coupling and losses is defined by C_{coup} and G_{coup}.

Chapter 4
Results and Discussion

The structure of the present chapter is divided into three parts regarding to each of the components(single inductor, differential inductor and transformer). Specific RLGC values for the models are found in the Appendix A, as well as the Q-factor of the devices, the model accuracy and the length of the designs.

4.1 Single inductor

As an initial step, a single microstrip-based inductor is analyzed. Both a 75Ω and a 50Ω line are considered, for which line width of $8\mu m$ and $16\mu m$ are used respectively.

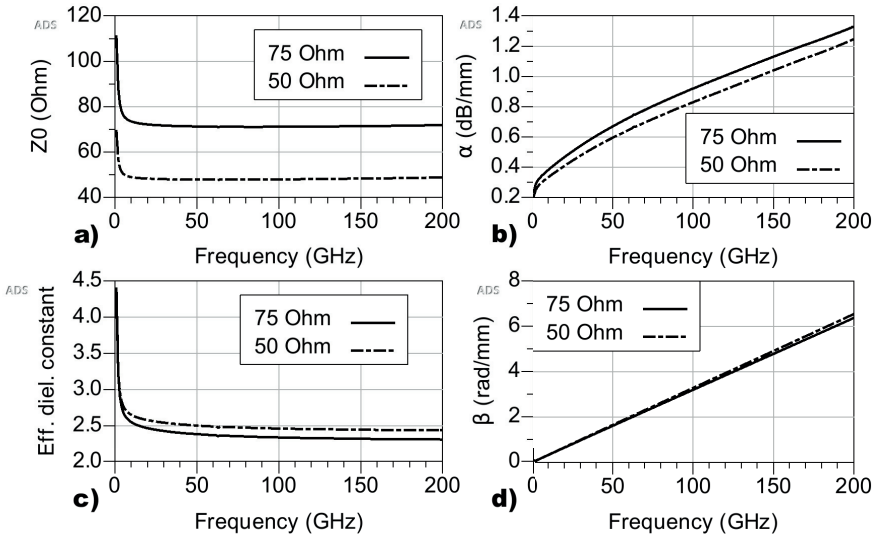

Figure 4.1: a) Characteristic impedance, b) attenuation constant, c) effective relative dielectric constant and d) phase constant for the 75Ω and 50Ω single inductors

The same BCB layer is used for both simulations but a wider line would produce more electric lines within the dielectric interlayer, so the effective relative

dielectric constant increases (Figure 4.1, **c)**). As expected, the slope of the phase constant increases with the width of the line and the attenuation constant decreases (Figure 4.1, **d)**) [10]. Also, the attenuation decreases linearly with the width (Figure 4.1, **b)**) as it is presented in [10], even though the value is slightly higher than expected.

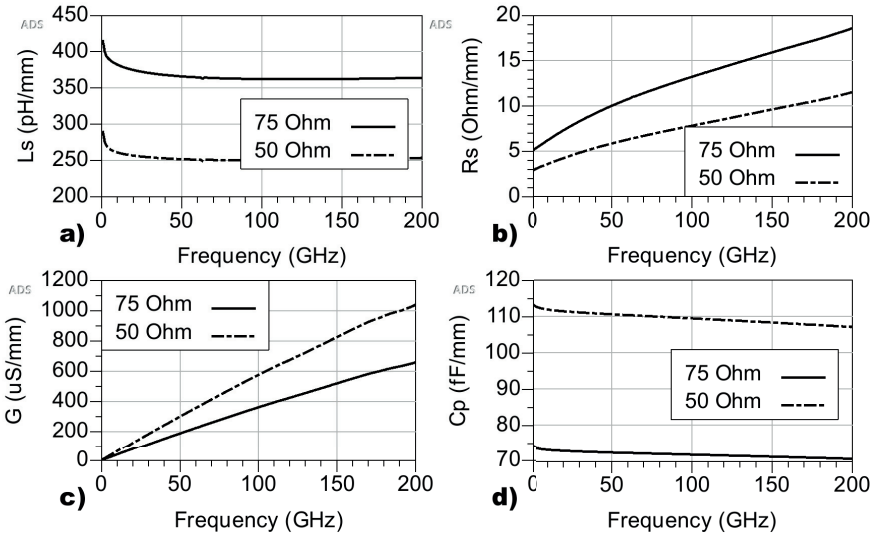

Figure 4.2: RLGC parameters for the 75Ω and 50Ω single microstrip inductors

Wider transmission lines have lower resistance per unit length since the cross-section is larger as can be translated into a decrease of the series resistance, an increase of the parallel conductance and a decrease of the series inductance [50]. This can be shown in Figure 4.2(**b)**, **c)** and **a)** respectively). Furthermore, when the area of the line increases, so do the area of the shunt capacitor that defines the parallel capacitance in Figure 4.2 **d)**.

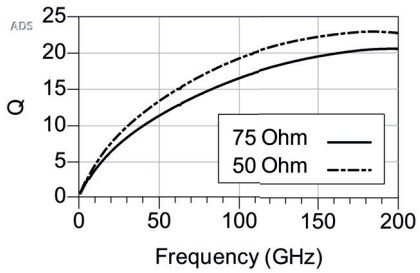

Figure 4.3: Q-factor for the 75Ω and 50Ω single microstrip inductors($100\mu m$)

As can be seen in Figure 4.3, a 50Ω line shows slightly higher Q-factor than the 75Ω line, and the peak of maximum value is displaced to lower frequencies

with the increase of the width. Note that the values for this models are similar to the ones obtained with lumped elements in ADS [43](Q=16.61). Increasing the width of the line reduces the losses and thus the Q-factor increases. On the other hand, not big differences can be seen around the interest band when the variation occurs in the length instead of the width. As can be seen in Figure 4.4, values for an increase and decrease of a 30% with respect to the initial value do not make a big difference in the Q-factor. However, at very high frequencies, the shorter the line, the higher the quality factor. On the other hand, longer lines implies higher inductance and higher resistance as well.

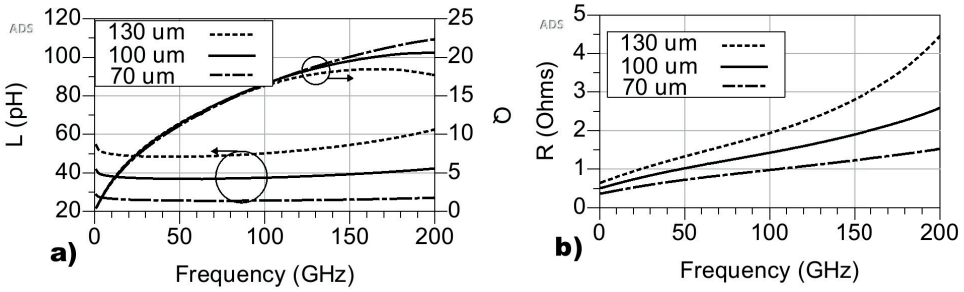

Figure 4.4: Inductance, Q-factor and resistance for the 75Ω single microstrip inductor (different length)

Figure 4.3 can be useful to show a comparison of the Q-factor for two lines with the same length but different width, however, if a comparison between two different inductors is needed, inductors with the same inductance have to be considered. Since the 50Ω line has lower inductance than the 75Ω, it is necessary to reduce the length of the 75Ω line in order to have similar values of inductance, as Figure 4.5 presents. It can be concluded that for a single microstrip inductor designed in this technology with a certain inductance, a 50Ω line has 17% higher Q-factor than a 75Ω line at 100 GHz.

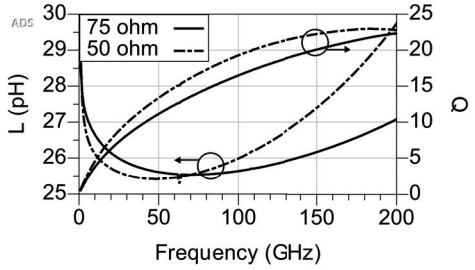

Figure 4.5: Inductance and Q-factor for the 75Ω(70μm) and 50Ω(100μm) single microstrip inductors

4.1.1 model

The 4-stage transmission line model presented in the previous chapter is followed to create a single microstrip inductor model. For the composition of the models, RLGC parameters are extracted from the lines. Also, DC resistance and the slope of the resistance and conductance graph shown in Figure 4.2 are used.

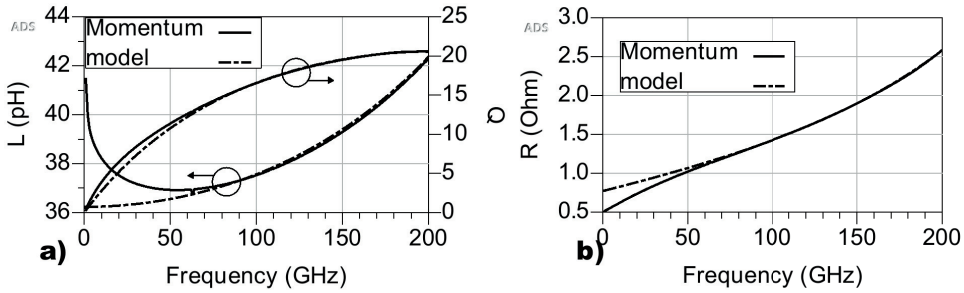

Figure 4.6: Q-factor, inductance and resistance for the 75Ω single microstrip inductor

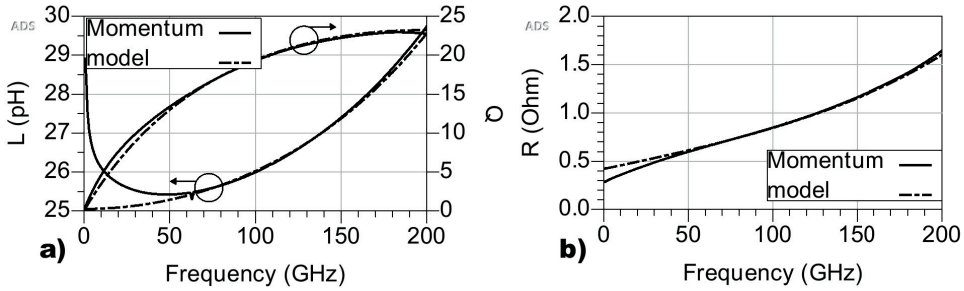

Figure 4.7: Q-factor, inductance and resistance for the 50Ω single microstrip inductor

Both lumped-element models almost overlap the graph of the Momentum model, as can be seen in figures 4.6 and 4.7, with a maximum of 1.3% of relative error within the W-band. The simplicity of this model makes that, even though it fits along the desired band, it is not possible to follow the behaviour at low frequencies. Some effects are not considered and, therefore, an overestimation of the losses and underestimation of the inductance for low frequencies can be seen. Apart from that, the model gives an accurate estimation of the single inductor.

4.2 Differential inductor

Once the transmission line is modelled and analyzed, a microstrip-based differential inductor can be defined. Throughout this section, not only the single-ended parameters (inductance, resistance and Q-factor) are measured, but the differential

ones as well. Single-ended parameters are calculated using Y-parameters, so when one port is being excited, the rest of the ports are shorted, and the opposite happens when differential parameters are calculated, since Z-parameters are used for that.

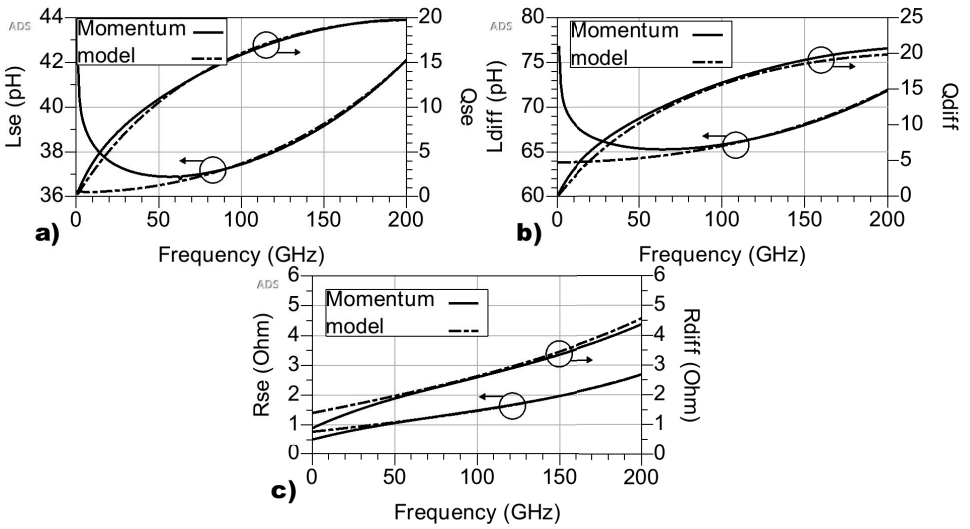

Figure 4.8: Q-factor, inductance and resistance for the differential 2F structure

The simplest structure used for a differential inductor consist on the 2 fingers (2F) structure: two parallel 75 Ω transmission lines joined by the centre tap. The shape around the centre tap is difficult to model since several 90º turns and sharp corners can cause variations on the characteristic of the inductor.

Since the model shown in 3.14 is pretty simple, the relative error for this lumped-element model increases from 1.3% in the transmission line case to a maximum of 2.3% with the 2F structure. Maximum relative error for the different models can be found in Appendix A. The fitting of the model can be shown in Figure 4.8, where, in the same way as the single transmission line, the model fits for the W-band but it does not follow the Momentum model for very low frequencies.

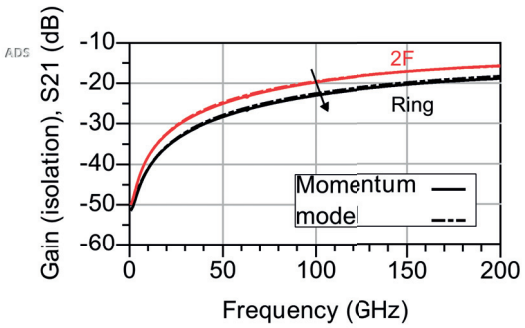

Figure 4.9: Gain(isolation) for the 75Ω differential inductors

With the goal of diminish the coupling and reduce the sharpness of the corners, a ring structure [45] is used. In the 2F case, the two parallel lines are separated by $20\mu m$ so a theoretical coupling coefficient of 0.06 would appear in the model, according to the coupling study. Taking into consideration only the coupling between parallel lines, with the use of the ring structure, it can be noticeable that the coupling between most of the parts are negligible since the distance between the sections that form the ring is more than $50\mu m$. Only coupling between the two sections next to the ports (sec_11 in Figure 3.15) occurs, where the distance is again $20\mu m$. Figure 4.9 shows the gain (isolation) for the two 75Ω structures, where it is possible to see the decrease in around 3.3 dB at 100 GHz when a ring structure is used. Considering that the centre tap is shorted, S_{21} represents the inductance between the two inductors, so is the mutual inductance, and thus, the inductive coupling, what is reduced when ring structure is used.

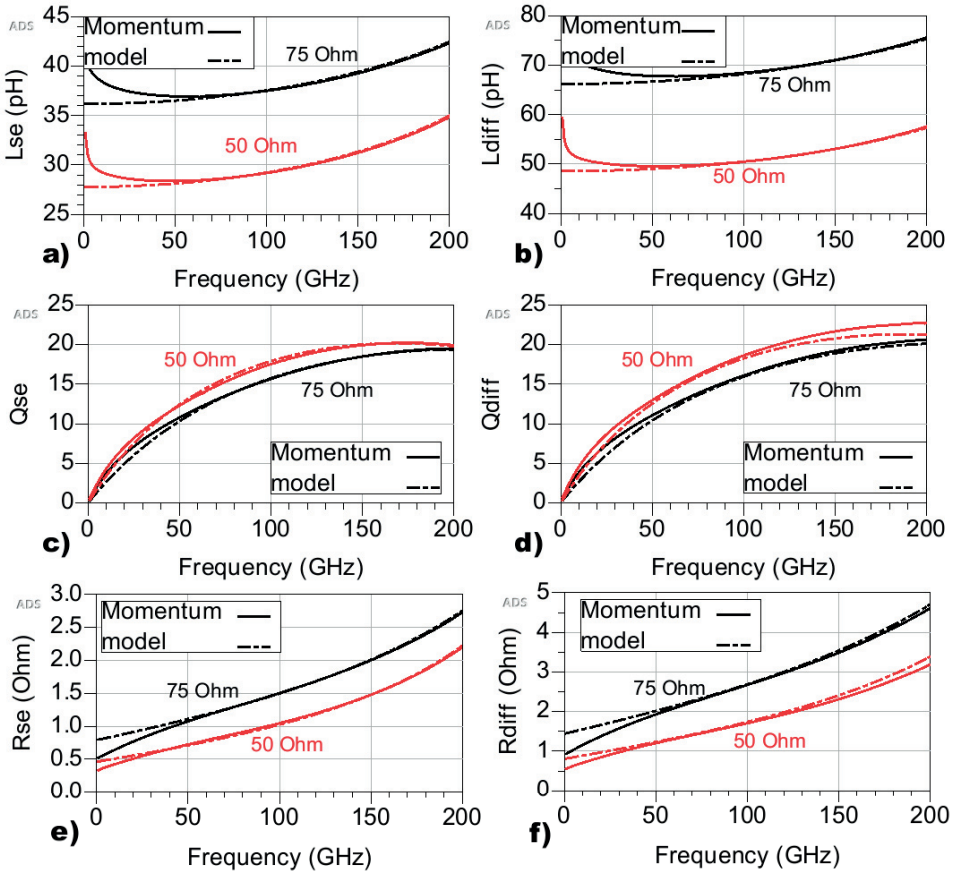

Figure 4.10: Inductance, Q-factor and resistance for the differential ring structure (50Ω and 75Ω)

Study was carried out in section 3.3.2 to choose a suitable ground extension in order to avoid the losses of fringe field, notwithstanding, differential structures are

not single transmission lines and different sections have different orientations. For that, it is possible that in sections next to the central tap (*sec_14* in Figure 3.14), some of the fringe fields may be lost, and the inductance can be reduced. Ring structure is not exempt from that. This is one of the reasons why L_s value is often reduced when the differential lumped-element model is tuned as it can be shown in Appendix A. Other reason may be the reduction of the effective electrical path.

Due to the use of Y-parameters, the results for the single-ended parameters in the differential inductors are similar to the ones shown in the previous section of the transmission line, as it is shown in figures 4.8 and 4.10. The figures shows how the model fits for the different widths of the transmission line, but still it is not possible to follow the trend at very low frequencies and, in some cases, at very high frequencies. Although the model could be more complex, the fitting shown in the graphs shows a maximum relative error of 1.9% for the 75Ω and a 2.8% for the 50Ω.

With the purpose of designing inductors with different inductances, a set of lengths are compared. For that, variations of +/-30% with respect to a $100\mu m$ long line are made. The results are similar to the ones made on the single inductor: inductance increase with the length and so do resistance. Q-factor remains the same value along the desired band, ignoring the length of the inductor.

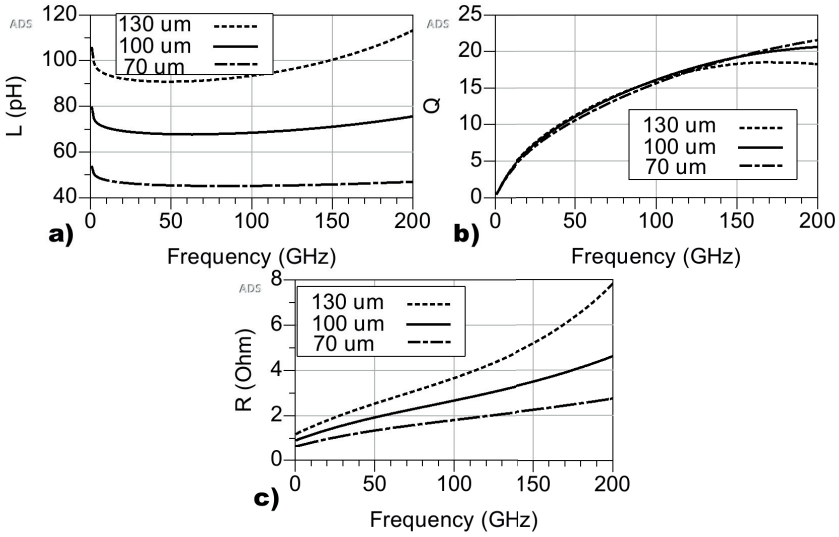

Figure 4.11: Q-factor and inductance comparison for the differential ring structure with different lengths (75Ω)

From observation, it can be concluded that a ring structure reduces significantly the coupling of the differential inductor and the Q-factor dependence on the width of the line is stronger than the one on the length.

4.3 Transformer

As it was above mentioned, transformers have been widely applied in mm-wave ICs [21]. DC isolation, impedance matching or balanced-to-unbalanced mode conversion are some of the applications for those devices. For that, different configurations are tested throughout this section, such as single ended to single ended or single ended to differential. Note that the two main transformers are based on the $100\mu m$ long transmission line, so the theoretical length is $200\mu m$ each winding. Due to layout considerations, the real length is larger, as can be seen in Appendix A (Figure A.1).

Designs

Apart from the two main transformers used in this thesis(75Ω and 50Ω), different designs are considered in this work. The only variation over 50Ω is 50ΩD, whose length is double than the 50Ω. For the 75Ω transformer, 5 variations are made: 75ΩNS, 75Ωh0, 75Ωv0, 75Ωinout and 75Ωoutin.

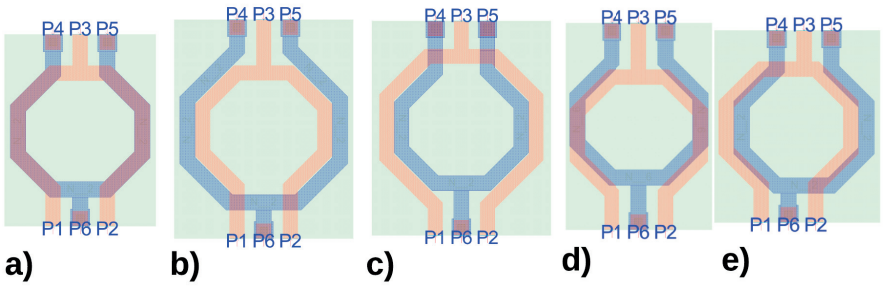

Figure 4.12: 75Ω transformers: a) completely overlapped b) in-out c) out-in d) v0 e) h0

75Ωv0 and 75Ωh0 refers to vertical and horizontal displacements in the layout, as it can be shown in Figure 4.12(d) and e)), while 75ΩNS refers to a transformer in which the raised ground plane, drawn in MET2, is removed. The main transformers and most of the designs are completely overlapped. With the purpose of study differences when the length of the windings are not equal, 75Ωinout and 75Ωoutin are described in figure 4.12(b) and c)). Note that the secondary winding (blue) is drawn in MET5 (top) and the primary (red) is drawn in MET3 (bottom).

In order to characterize a transformer, several measurements have to be taken. Some of them are defined below.

DC resistance

Although an ideal transformer behaves like two non-coupled wires when it is not receiving any excitation, a real transformer presents some resistance when no AC current is flowing through it. Table 4.1 below shows the values of the DC resistance

for the two main transformers (75Ω and 50Ω). The lower DC resistance of the 50Ω shown in table 4.1 can be explained by the wider microstrip line.

Transformer	primary winding	secondary winding
75Ω	0.978Ω	0.97Ω
50Ω	0.61Ω	0.589Ω

Table 4.1: DC resistance of the transformer

Impedance ratio

The turns ratio of the transformer was already explained in section 2.1.1. The impedance ratio can be defined as n^2, being n the turns ratio, according to equation 2.6. The value refers to the transformation the device provides in terms of electrical characteristics, which is used to calculate it based on Z-parameters. Three different 75Ω transformers are compared in table 4.2.

As expected, when the two windings are completely overlapped the value is near 1 for both the 75Ω and the 50Ω($n = 1.082$) transformers. What is more, when the secondary winding is larger than the primary (in-out) this value increases and it decreases when the primary is the largest one (out-in). When the length of one of the windings increases it has the same effect as increasing the "number of turns", defined as N_x in equation 2.6.

75Ω	Overlapped	in-out	out-in
n	1.07	1.158	0.989
Impedance ratio (n^2)	1.145	1.341	0.978

Table 4.2: Impedance ratio for 75Ω transformers

Amplitude and phase unbalance

Following the equations and expressions explained in section 2.1.1 it is possible to get an amplitude unbalance of 1.375 dB for the 75Ω transformer and a 3.98 dB for the 50Ω. Furthermore, the fact that the 50Ω transformer is less symmetric than the 75Ω one is confirmed when the phase unbalance is 1.933º for the 75Ω and 4.707º for the 50Ω. Since the designs are almost symmetrical, non-symmetrical differences in the mesh may cause this asymmetry.

Self-inductance and Q-factor

Inductance and Q-factor can be measured in both windings of the transformer to characterize it as it was explained in section 2.5. The results of the measurements of the 50Ω and the 75Ω based on $100\mu m$ lines are shown in Figure 4.13.

The performance of the transformers is limited by their self-resonance frequency (SRF) shown in Figure 4.13, a) and c). It is easy no notice that a resonance occurs

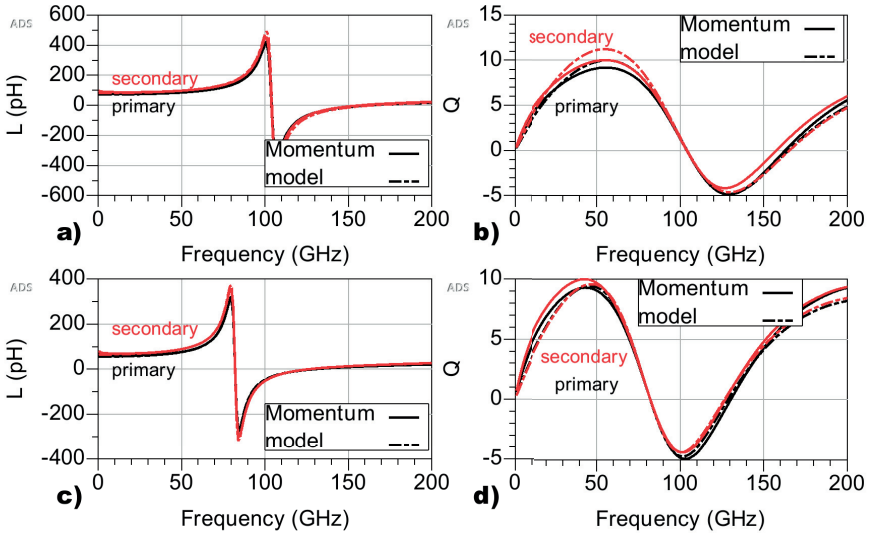

Figure 4.13: Q-factor and inductance for the transformer a)&b)75Ω, c)&d)50Ω with a single-ended to single-ended configuration

around 100 GHz for the 75Ω transformer and around 80 GHz for the 50Ω in a single-ended to single-ended configuration without bias. Furthermore, the most efficient use of the transformer can be defined as the range in which the Q-factor is maximum, that should be around half the SRF. It can be seen that the model follows the trend for the inductance and the Q-factor.

Coupling coefficient

As said in section 2.1.1, two ways to define the coupling are considered: capacitive-inductive or resistive-reactive. Section 2.3 defines the model of the transformer as two differential ring inductors placed at the top to each other, so capacitive coupling is added as real capacitors (considering losses) and the component MUTIND of ADS Keysight is used to consider the inductive coupling.

Transformer	75Ω	50Ω	50ΩD	75ΩNS	75Ωh0	75Ωv0
$C_{coup}(fF)$	19.2	45.6	80	21.6	10.4	12.8
k	-0.81	-0.79	-0.79	-0.95	-0.61	-0.59

Table 4.3: Inductive and capacitive coupling between the two windings of the transformers. C_{coup} refers to the capacitance between the windings and k is the inductive coupling coefficient

Table 4.3 shows both the capacitive and the inductive coupling used in the model of the transformer, where the components are the ones defined in image 3.16. The two main transformers and some variations of them are considered in this table.

The ground plane acts as a shield that blocks the magnetic flux with the purpose of reducing the substrate effect, as said in section 2.1.1, thus the removal of this plane will increase the inductive coupling in the transformer. Nevertheless, the absence of ground plane decreases the resonance from 100 GHz to 60GHz. The displacement shown in 75Ωh0 and 75Ωv0 provokes a reduction on the capacitive coupling, since the two windings are not completely overlapped and the effective area of the capacitor between them is, hence, reduced. Also, the fact that the secondary and the primary windings are not aligned can reduce the magnetic flux through them, increasing the flux leakage and reducing the inductive coupling, as it is shown in table 4.3. The values obtained in the models are within one of the typical ranges for a k-factor in monolithic transformer designs ($0.6 \leq \mid k \mid \leq 0.95$) [31].

An alternative way to describe the coupling coefficient is presented below. It is possible to describe the coupling in a resistive-reactive way as well. The common shape of those coefficients presents, in the self-resonant frequency, a maximum in the resistive part and a resonance in the reactive part [32]. Figure 4.14 shows how k_{Re} reach its maximum when the resonance takes effect, as well as k_{Im} has a resonant peak at that frequency.

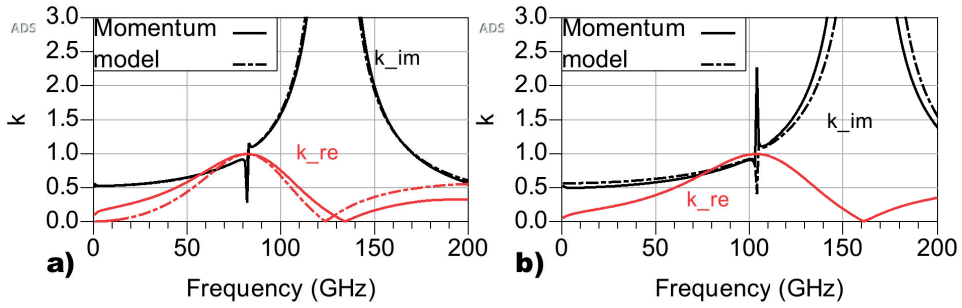

Figure 4.14: Real and imaginary coupling coefficients for a) a 50Ω and b) a 75Ω transformer

Frequency range and insertion loss

Insertion losses are often the main characteristic of a transformer since it gives information about the attenuation of the signal and the energy transfer. The way of measuring it is through S_{21} (gain) that is calculated directly by ADS. Depending on the maximum value of insertion losses that our system is designed for, the frequency range may vary. Along this thesis, the maximum acceptable value will be 1 dB, that it will define the bandwidth in which the transformer can work.

An example of this measuring can be seen in Figure 4.15, where the gain of the 50Ω transformer can be shown. From this figure it can be extracted that the peak of the gain occurs at 94 GHz and the band starts at 87 GHz and ends at 101 GHz, so a bandwidth of 14 GHz can be achieved. As it was explained in section 2, one key characteristic of a transformer is the maximum available gain, $Gmax$ in the figure. For the 50Ω transformer it looks that in a single-ended to single-ended configuration without bias it matches around the desired frequency, 100 GHz. Even

though, as it was presented in Figure 4.13, the transformer behaves like that up to approx. 80 GHz, so it is not completely trustworthy.

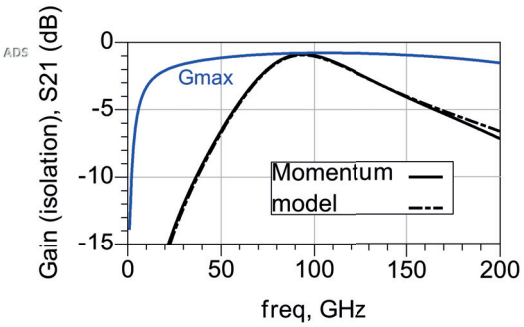

Figure 4.15: Gain of a 50Ω transformer for a single-ended to single-ended configuration without bias

4.4 Configurations

As it was said above, depending on the purpose, a transformer will be connected in a different way. Some of those configurations are shown in Figure 4.16. If one of the windings of the transformer is connected in a single-ended model that means one of the terminals is connected to ground, while the other one is connected to the input or output. On the other hand, a differential connection requires both terminals of the winding to be connected to the input or output. Furthermore, the windings can be biased or not. Since a bias signal is often a DC voltage, when it comes to measure it using S-parameters, a grounded port is used instead. Differential ports often use biased central tap, as can be shown in [43]. Throughout this subsection, some transformers will be tested using different configurations.

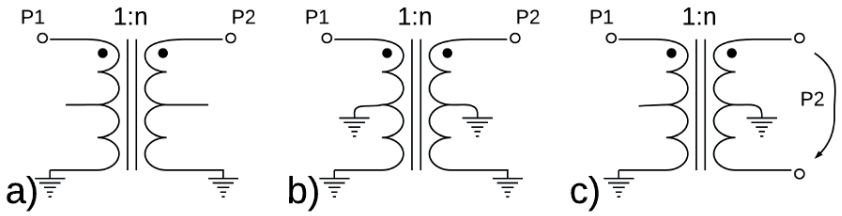

Figure 4.16: Transformer configurations: a) single-ended to single-ended b) single-ended to single-ended (with bias) and c) single-ended to differential

4.4.1 single-ended to single-ended

The simplest configuration in which a transformer can be used is a single-ended to single-ended configuration. The two main transformers of the thesis (50Ω and a 75Ω based on a 100μm long line) response can be shown in Figure 4.17 and 4.19.

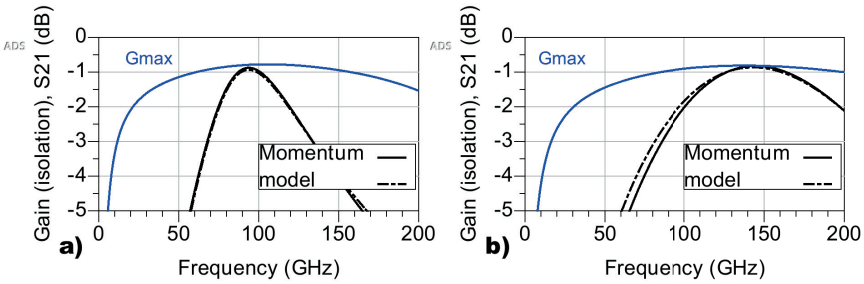

Figure 4.17: Gain of a) a 50Ω and b) a 75Ω transformer for a single-ended to single-ended configuration without bias

When no bias is required, both transformers offers a range of frequencies in which the value of S_{21} is higher than -1dB. The useful band for the 50Ω is located at lower frequencies than the 75Ω, even though the range is narrower. Note that the 50Ω has its maximum value around 95 GHz (close to the desired frequency) and its frequency range extends from 87 to 101 GHz, while the 75Ω has its range between 126 and 164 GHz, that is wider but further from 100 GHz. The frequency ranges can be summarized in table 4.4.

Transformer	bandwidth(GHz)	max available bandwidth(GHz)
50Ω	87-101(14)	61-157(96)
75Ω	126-164(38)	85-199(114)

Table 4.4: Frequency ranges of a) a 50Ω and b) a 75Ω transformer for a single-ended to single-ended configuration without bias

The maximum gain defines the potential maximum bandwidth and frequency range that those transformers can reach with this configuration if all its ports were perfectly matched. Although the 50Ω transformer seem to be suitable for a single-ended to single-ended purpose all over the W-band, it is important to notice that, as shown in Figure 4.13, both transformers have a self-resonance around 80 or 100 GHz, so the transformers only behave like transformers up to (less than) that frequency. In addition, it is possible to conclude that a wider transformer may have a useful band at lower frequencies than a narrower one. Another way to move the band to lower frequencies it is to increase the length of the windings, as it is presented in Figure 4.18. Nevertheless, the self-resonant frequency is reduced too when the length increases so the problem persist.

Based on Figure 4.18, it is possible to assert that, for a single-ended to single-ended configuration without bias, the frequency useful band moves to lower frequencies when the length or the width of the transformers are increased. Also, the

self-resonant frequency decreases with the length or the width.

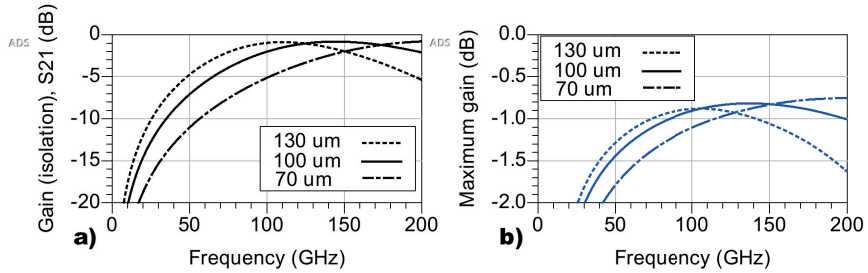

Figure 4.18: a) Gain and b) maximum available gain of a different length 75Ω transformers for a single-ended to single-ended configuration without bias

Bias is usually required in some RFICs, so a grounded central tap is considered to have the results obtained in figures 4.19 and 4.22. Grounding the central tap in a single-ended to single-ended configuration, half of the transformer is shorted so technically only half of the transformer is "transferring energy". That is translated into a displacement to higher frequencies. Without any matching circuit, the $100\mu m$ line based transformers are not useful for this purpose as shown in Figure 4.19, however, with the optimal matching it is possible to have a bandwidth which lower limit is around 77 GHz for the 50Ω and 102 GHZ for the 75Ω. The self-resonant frequency is pushed to higher frequencies as well, 160 GHz for the 50Ω and higher than 200 for the 75Ω.

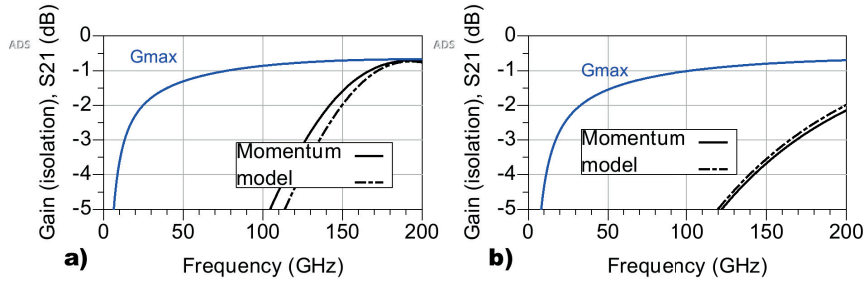

Figure 4.19: Gain of a) a 50Ω and b) a 75Ω transformer for a single-ended to single-ended configuration with bias

Every conducted simulation during the present document has been using 50-Ω terminals to get the S-parameters. For that, a matched port for a specific frequency will be translated in a Smith chart as this frequency hitting the central point of the chart, 50 Ω in this case. Figure 4.20 represents the input reflection coefficient of the input(S_{11}) and output(S_{22}) ports for the transformers. The point that corresponds to the desired frequency (100 GHz) is not even close to the centre of the chart, so a matching circuit it is necessary.

Variations are made over the simple transformers in order to obtain better results along this band. While in the configuration without bias an increase of the

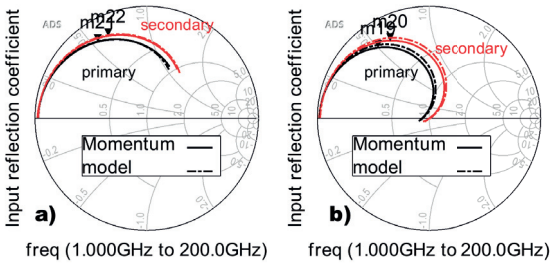

Figure 4.20: Input reflection coefficient of a a)75Ω and a b)50Ω transformer for a single-ended to single-ended configuration with bias. Marks at 100 GHz

length was translated into a displacement of the band to lower frequencies, when a bias central tap is used, that increase of the length implies an increase of the gain and thus, of the bandwidth, as presented in Figure 4.21. A transformer based on a 130Ω line will offer the best result inasmuch as the maximum gain showed in Figure 4.21,b) presents a maximum available bandwidth that starts around 85 GHz. The self resonant frequency is placed around 160 GHz, therefore, with the correct matching circuit, a bandwidth between 85 and 160 GHz can be achieved.

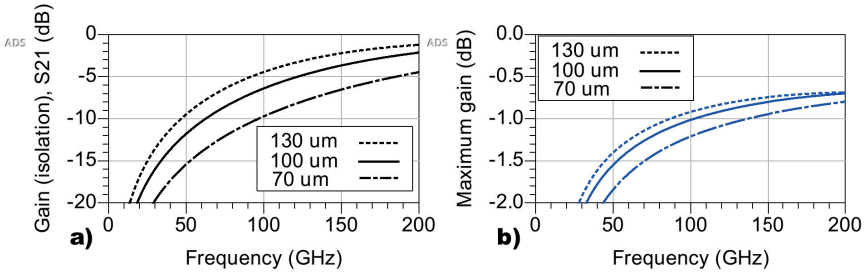

Figure 4.21: a) Gain and b) maximum available gain of a different length 75Ω transformers for a single-ended to single-ended configuration with bias

Since grounding the central tap will reduce to the half the "effective length", increasing to double may sound reasonable, so the 50ΩD transformer is tested here. Also, removing the raised ground will increase the inductive coupling and the energy transfer, that is why 75ΩNS is probed. Figure 4.22 show both the isolation gain and the maximum gain for those two variations in comparison with the original versions.

When ground is removed, maximum gain increases and then the available bandwidth too as it is shown in Figure 4.22, a). The self-resonance frequency for this transformer is placed around 120 GHz, so values from 26 GHz (lower available band limit) to around 100 GHz are suitable to be used with a suitable matching. On the other hand, the increment of the length is translated into a displacement to lower frequencies, as it is presented in Figure 4.22, b). In the case of the 50ΩD the

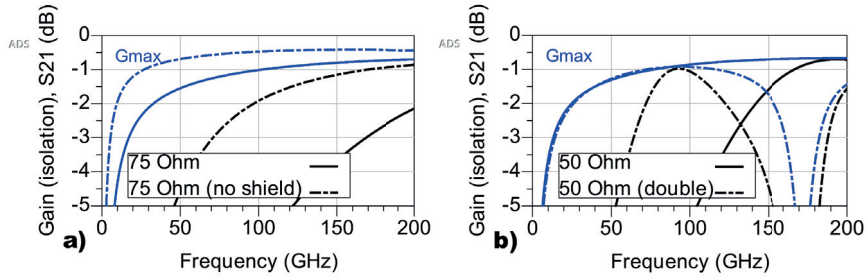

Figure 4.22: Gain of a) a 75ΩNS and b) a 50ΩD transformers in comparison with the simple ones for a single-ended to single-ended configuration with bias

self-resonant frequency at 60 GHz makes this transformer only useful up to a too low frequency. With a high self-resonant frequency and a wide band, the 75ΩNS can be interesting to explore, but difficult to model, as there are substrate effects. FEM simulation would be more suitable for this transformer.

4.4.2 single-ended to differential

In terms of measuring the single-ended to differential configuration showed in Figure 4.23, a back-to-back configuration is often used. This configuration allows to have a measuring of the gain in the same way as it was done in a single-ended to single-ended configuration. -2dB will be the limit instead of -1 dB, since two transformers are connected in series, as shown in Figure 4.23.

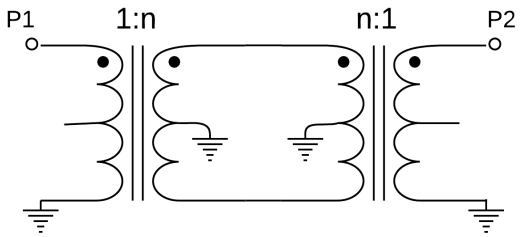

Figure 4.23: Back-to-back configuration

As it was done with the single transmission line, different lengths are tried for the transformer. A displacement in frequencies when the length increases can be seen in Figure 4.18, while when the central tap is biased, the variation of the length is translated into an increment on the gain as Figure 4.21. The behaviour for the single-ended to differential configuration can be explained as a mix between figures 4.18 and 4.21, since a displacement to low frequencies and an increase of the gain can be seen when the length increases in Figure 4.24. It is possible to conclude from Figure 4.24 that the initial transformers cannot work in a single

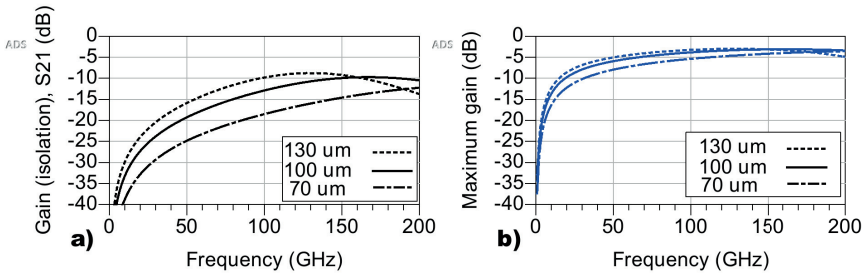

Figure 4.24: Gain of a different length 75Ω transformers for a single-ended to differential configuration (back-to-back)

ended to differential configuration since the graphs of the maximum gain for both does not reach the -2 dB level.

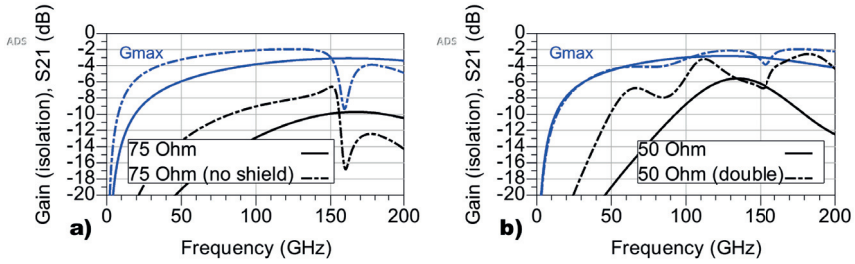

Figure 4.25: Gain of a) a 75ΩNS and b) a 50ΩD transformers in comparison with the simple ones for a single-ended to differential configuration (back-to-back)

Two more variations are taken into account: 75ΩNS and 50ΩD. By removing the raised ground plane in the 75Ω transformer this maximum gain increases the same way as it did in the single-ended to single-ended with bias above. A maximum available bandwidth of 25 GHz from 110 to 135 GHz can be achieved. When a 50Ω transformer doubles its length, non-uniform behaviour is shown in Figure 4.25, b). Nonetheless, in the frequency range from 169 to 185 GHz, a 16 width bandwidth can be achieved.

Chapter 5
Conclusions

The aim of this thesis was to explore the suitability in the design of mm-wave on-chip differential inductors in the W-band using the technology defined in the Nanoelectronics Group Student Library. Several variations of single and differential inductors and transformers are tested and transmission line-based lumped-element models are defined for the most general designs. Throughout this work, ADS Keysight software has proved to be a powerful and efficient tool in terms of layout design in mm-wave regime, allowing different types of simulations such as Momentum μW to provide a complete characterization of the designs.

Differential inductors designed in this work achieve relatively high Q-factors at 100 GHz shown in table A.2 that allows its use in RF applications, as well as the possibility to create a transformer based on those devices. Furthermore, the study of different configurations for transformers has revealed the possibility of its use in several applications.

To conclude, it has been possible to achieve all goals set out for the thesis. The designs show promising results and models for them are described. Thus, it is possible to assert that the technology used throughout this document is suitable for the design of mm-wave inductors operating in the W-band.

5.1 Future work

Although all the goals are achieved, the wide scope of this work makes it easy to extend. Future work could include some of the following points:

- The relative error obtained in the model increases drastically when it comes to the transformer, as shown in table A.6, so a more exhaustive and detailed design of the model could be done, taking into account some effects such as radiation that are not considered in this document.
- A deeper study of the skin effect and the fringe field.
- Use of more complex mesh to obtain more accurate results. The selected mesh settings were limited by simulation time and the available hardware, so a balance between complexity of the mesh and time consumption was made. The difficulties to measure losses can be shown in Figure A.2, where the mesh settings used in this work are compared with a more complex one.

- FEM simulation instead of Momentum μW for transformers, since FEM is more suitable for 3D structures.

References

[1] E. Sharma ,*Design of millimeter wave VCO based on slow-wave transmission lines, master thesis*, June 2017

[2] G. Liu, R. Berenguer, Y. Xu, *A MM-Wave Configurable VCO Usign MCPW-Based Tunable Inductor in 65-nm CMOS*, IEEE transactions on circuits and systems-II: express briefs, Vol. 58, No. 12, December 2011.

[3] M. Danesh, J. R. Long, *Differentially Driven Symmetric Microstrip Inductors*, IEEE transactions on microwave theory and techniques, Vol. 50, No. 1, January 2002.

[4] M. T. Reiha, T. Choi, J. Jeon, S. Mohammadi, L. P. B. Katehi, *High-Q Differential Inductors for RFIC Design*, 33rd European Microwave Conference Proceedings, October 2003.

[5] S. Nehra, P.K. Ghosh, E. P. Soni, *Design and analysis of differential floating inductor for filter*, International Conference on Electrical, Electronics, and Optimization Techniques, 2016

[6] K. Rasouli, A. Nouri, M. Sabaghi, A. M. Kordalivand, M. A. Far, *Design and simulation of differential active inductor with 0.18 μm CMOS Technology*, IEEE International Conference on System Engineering and Technology, June 2011

[7] K. Bellows, *Advantages and Disadvantages of Active Inductors on Chip over Monolithic Inductors*, Department of Electrical and Computer Engineering, Texas A&M University, December 2013

[8] J. A. del Alamo, *Nanometre-scale electronics with III–V compound semiconductors*, Nature 479, pp 317–323, 2011

[9] Nano Electronics – Lund University, https://portal.research.lu.se/portal/en/organisations-researchgroups/nano-electronics(c468b4fc-73f8-4b05-b7f8-5c6cfce2b930).html

[10] S. Andric, L. Ohlsson, L. Wernersson, *Low-Temperature Front-Side BEOL Technology with Circuit Level Multiline Thru-Reflect-Line Kit for III–V MOSFETs on Silicon*, 92nd ARFTG Microwave Measurement Conference (ARFTG), January 2019.

[11] UY1: Self-Inductance & Inductors,
https://www.miniphysics.com/uy1-self-inductance-inductors.html

[12] Reference Designer. Chapter 5: Inductance,
http://referencedesigner.com/books/si/inductance.php

[13] Inductance and Magnetic Energy, Chapter 11.1 - Mutual inductance, MIT,
http://web.mit.edu/viz/EM/visualizations/notes/modules/guide11.pdf

[14] What is Self-Resonant Frequency,
https://www.everythingrf.com/community/what-is-self-resonant-frequency

[15] J. Borremans, M. Dehan, K. Scheir, M. Kuijk, P. Wambacq, *VCO design for 60 GHz applications using differential shielded inductors in 0.13 μm CMOS*, IEEE Radio Frequency Integrated Circuits Symposium, June 2008

[16] P. You, K. Huang, T. Huang, *56 GHz CMOS VCO Integrated with a Switchable Non-uniform Differential Transmission-Line Inductor*, European Microwave Conference (EuMC), October 2009

[17] Reference Designer. Chapter 9: Transmission line,
http://referencedesigner.com/books/si/Transmission_Line.php

[18] N. Troedsson, J. Wernehag, H. Sjöland, *Differential Measurement and Parameter Extraction of Symmetrical Inductors*, Department of Electroscience, Lund University, 2005

[19] J. B. Calvert, *Inside transformers*, University of Denver, January 2001, https://web.archive.org/web/20070610032645/http://www.du.edu:80/~jcalvert/tech/transfor.htm

[20] B. Leite, E. Kerhervé, J. Bégueret, *Design and Characterization of CMOS Millimeter-Wave Transformers*, SBMO/IEEE MTT-S International Microwave and Optoelectronics Conference (IMOC), November 2009

[21] D. Hou, W. Hong, W. L. Goh, Y. Z. Xiong, M. A. Arasu, J. He, J. Chen, M. Madihian, *Distributed Modeling of Six-Port Transformer for Millimeter-Wave SiGe BiCMOS Circuits Design*, IEEE Transactions on Microwave Theory and Techniques, Vol. 60, No. 12, December 2012

[22] F. Huang, J. Lu, Y. Zhu, N. Jiang, X. Wang, Y. Chi, *Effect of Substrate Parasitic Inductance on Silicon-Based Transmission Lines and On-Chip Inductors*, IEEE Electron Device Letters, Vol. 28, No. 11, November 2007.

[23] T. Das, S. Chatterjee. *Performance of periodic grooves on harmonic rejection in C band folded edge coupled microstrip band pass filters.* https://www.researchgate.net/publication/312628412_Performance_of_periodic_grooves_on_harmonic_rejection_in_C_band_folded_edge_coupled_microstrip_band_pass_filters October, 2016

[24] C. B. Sia, K. W. Chan, C. Q. Geng, W. Yang, K. S. Yeo, M. A. Do, J. G. Ma, S. Chu, K. W. Chew, *An Accurate and Scalable Differential Inductor Design Kit*, IEEE Conference on Microelectronic Test Structure, Vol. 17, March 2004.

[25] , Y. Moisiadis, S. Stefanou, P. Papadopoulos, *Integrated Inductor Compact Modeling Methodology*, Journal of Engineering Science and Technology Review, June 2015.

[26] H. Tu, T. Yang, H. Chiou, *Low phase noise VCO design with Symmetrical Inductor in CMOS 0.35-μm Technology*, Asia-Pacific Microwave Conference Proceedings, December 2005.

[27] D. M. Pozar, *Microwave engineering*, 4th Edition, John Wiley & Sons, 2012.

[28] A. Czyk, S-parameters tutorial, `https://incompliancemag.com/article/s-parameters-tutorial-part-i-fundamental-background/`

[29] Smith Charts, `http://www.antenna-theory.com/tutorial/smith/chart.php`

[30] *S-Parameter Design - Application Note*, `http://literature.cdn.keysight.com/litweb/pdf/5952-1087.pdf`

[31] W. Simbürger, A. L. Scholtz, *Design of Monolithic Integrated Lumped Transformers in Silicon-based Technologies up to 20 GHz*, December 2000.

[32] D. Sengupta, S. Gaskill, A. Weisshaar, *A Lumped Element Circuit Model for Monolithic Transformers in Silicon-based RFICs*, IEEE 23rd Conference on Electrical Performance of Electronic Packaging and Systems, October 2014.

[33] O. El-Gharniti, E. Kerhervé, J. Bégueret, P. Jarry, *Modelin of Integrated Monolithic Transformers for Silicon RFIC*, 11th IEEE International Conference on Electronics, Circuits and Systems, Decemeber 2004.

[34] K. T. Ng, B. Rejaei, J. N. Burghartz, *Substrate Effects in Monolithic RF Transformers on Silicon*, IEEE Transactions on Microwave Theory and Techniques, Vol. 50, No. 1, January 2002.

[35] Application Note on Transformers, Mini-Circuits, `https://www.minicircuits.com/app/AN20-002.pdf`.

[36] ADS webpage, `https://www.keysight.com/en/pc-1297113/advanced-design-system-ads`

[37] Momentum basics - ADS 2009 Update 1, `http://edadocs.software.keysight.com/display/ads2009U1/Momentum+Basics`

[38] Theory of Operation for Momentum - ADS 2009 Update 1, `http://edadocs.software.keysight.com/display/ads2009U1/Theory+of+Operation+for+Momentum#TheoryofOperationforMomentum-1107072`

[39] FEM Simulator basics - ADS 2009 Update 1, `http://edadocs.software.keysight.com/display/ads2009U1/FEM+Simulator+Basics`

[40] S. Costanzo, I. Venneri, G. Di Massa, A. Borgia, *New technologies and antenna design concepts at millimeter-wave bands*, 3rd European Conference on Antennas and Propagation, March 2009.

[41] X. Huo, K. J. Chen, P. C. H. Chan, *Silicon-Based High-Q Inductors Incorporating Electroplated Copper and Low-K BCB Dielectric*, IEEE Electron Device Letters, Vol. 23, No. 9, September 2002.

[42] Q. Pan, L. Sun, C. P. Yue, *Differential Stacked Spiral Inductor and Transistor Layout Designs for Broadband High-Speed Circuits*, IEEE International Symposium on Radio-Frequency Integration Technology, August 2014.

[43] X. Yan, *A 100GHz Millimeter-Wave Voltage-Controlled Oscillators in III-V Nanowire Technology*, Master's Thesis, LTH, Lund University, May 2019.

[44] H. Y. D. Yang, *Design Considerations of Differential Inductors In CMOS Technology for RFIC*, IEEE Radio Frequency Integrated Circuits Symposium, June 2004.

[45] D. I. Sanderson, "High Q Monolithic Inductors For Use In Differential Circuits", United States Patent 7,259,625 B2, Aug. 21, 2007.

[46] Recommendations for Port Setup When Using ADS Momentum and Modelithics Models - Application Note, http://literature.cdn.keysight.com/litweb/pdf/5992-0415EN.pdf

[47] Inductor EM simulation: 1-port or 2-port?, http://muehlhaus.com/support/ads-application-notes/inductor-em-ports

[48] Keysight ADS - Mesh, http://literature.cdn.keysight.com/litweb/pdf/ads2008/mom/ads2008/Mesh.html

[49] Measurement of Skin Effectsusing the Bode 100, https://www.omicron-lab.com/fileadmin/assets/Bode_100/Articles_UseCases/Article_Skin_Effect_v1_0.pdf

[50] S. Ahyoune, J. Sieiro, M. N. Vidal, J. M. López-Villegas, *Skin Effect Formula for Metal Strips in LaminatedSubstrates*, 32nd Conference on Design of Circuits and Integrated Systems (DCIS), November 2017.

[51] P. Findley, G. A. Rezvani, J. Tao, *Novel Differential Inductor Design for High Self-Resonance Frequency*, IEDM Technical Digest. IEEE International Electron Devices Meeting, December 2004.

[52] M. Rafeequdin, 'Power Systems: In which case does nominal "T" and nominal "PIE" are used and which one is superior for which kind of analysis?', https://www.quora.com/Power-Systems-In-which-case-does-nominal-T-and-nominal-PIE-are-used-and-which-one-is-superior-for-which-kind-of-analysis

[53] Mutual Inductors - ADS 2009, http://edadocs.software.keysight.com/display/ads2009/Mutual+Inductors

[54] S. C. Wang, G. W. Huang, S. D. Wu, A. S. Peng, M. H. Cho, *Monolithic Transformer Modeling Based on the 4-port Characterization Technique*, International Conference on Solid State Devices and Materials, 2003.

[55] J. R. Long, *Monolithic Transformers for Silicon RF IC Design*, IEEE Journal of Solid-State Circuits, Vol. 35, No. 9, September 2000.

Appendix A
Extra material

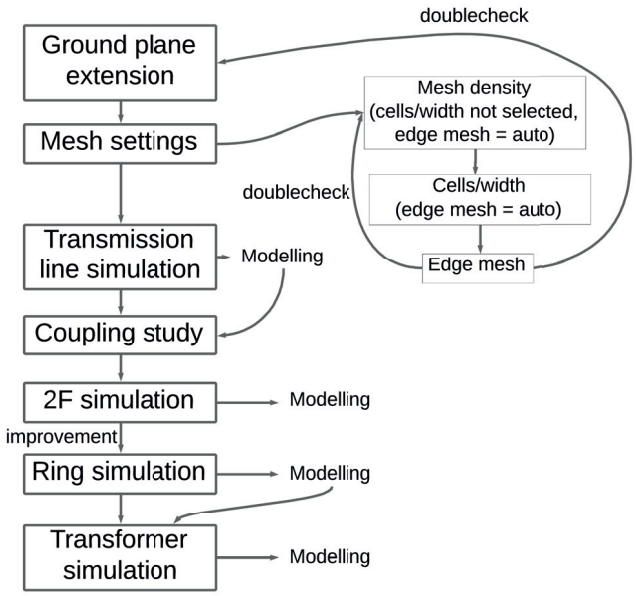

Figure A.1: Flux diagram of the simulations done along this work

	Single	Differential	Transformer(1 winding)
75Ω	$100\mu m$	$200\mu m$	$216\mu m$
50Ω	$100\mu m$	$217\mu m$	$249\mu m$
50ΩD	$200\mu m$	-	$508\mu m$
75Ω+30%	$130\mu m$	$260\mu m$	$270\mu m$
75Ω-30%	$70\mu m$	$140\mu m$	$158\mu m$
75Ω inout	-	-	$232\mu m/268\mu m$
75Ω outin	-	-	$268\mu m/232\mu m$

Table A.1: Length of the inductors used in this thesis

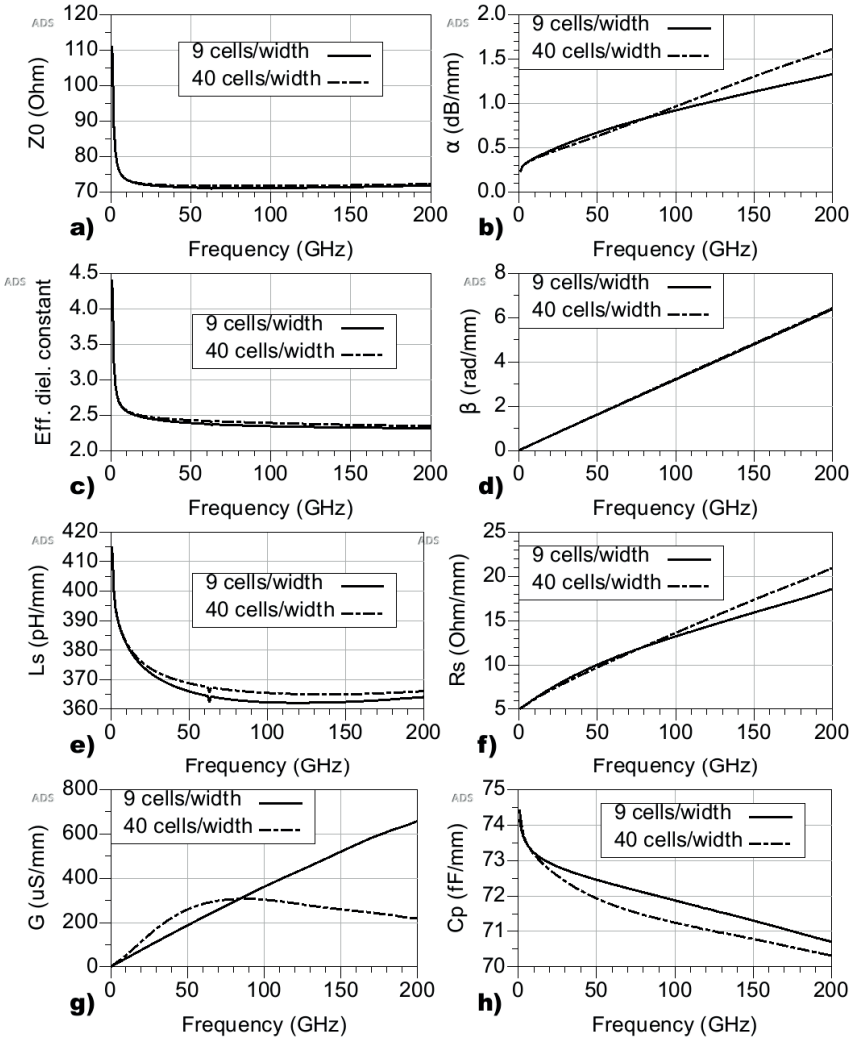

Figure A.2: a) Characteristic impedance, b) attenuation constant, c) effective relative dielectric constant, d) phase constant, e) inductance, f) resistance, g) conductance and h) capacitance for the transmission line used in this work. Continuous line represents the mesh settings used in this thesis (mesh density = 100 cells/wavelength, edge mesh = 0.25 um and transmission line mesh = 9 cells/width) and discontinuous line represents a more accurate mesh (mesh density = 100 cells/wavelength, edge mesh = 0.05 um and transmission line mesh = 40 cells/width)

Component	Q-factor
75Ω microstrip line	16.541
50Ω microstrip line	19.272
75Ω 2F differential inductor	15.901
75Ω Ring differential inductor	16.092
50Ω Ring differential inductor	18.612

Table A.2: Q-factor of the single and differential inductors

Component	Q-factor (1st winding)	Q-factor (2nd winding)
75Ω Transformer	13.974	15.076
50Ω Transformer	14.576	15.358

Table A.3: Differential Q-factor of the transformers

Inductor	Single	2F	Ring	Transformer (1st winding)	Transformer (2nd winding)
$L_s(pH)$	36.23	33.2	32.9	33.15	37.9
$R_s(\Omega)$	1.322	1.3	1.3	1.315	1.2618
$C_p(fF)$	7.187	6.4	6.7	6.18	4.57
$G(\mu S)$	36.1	36.1	36.1	36.4	28.23

Table A.4: RLGC parameters for every inductor structure (75Ω)

Inductor	Single	Ring	Transformer (1st winding)	Transformer (2nd winding)
$L_s(pH)$	25.05	22.2	22.2	26.7
$R_s(\Omega)$	0.7819	0.8	0.85	0.85
$C_p(fF)$	10.94	10.5	8.7	3.6
$G(\mu S)$	57.6	57.6	59.1	42.69

Table A.5: RLGC parameters for every inductor structure (50Ω)

Component	Relative error
75Ω microstrip line	1.31%
50Ω microstrip line	0.5%
75Ω 2F differential inductor	2.32%
75Ω Ring differential inductor	1.93%
50Ω Ring differential inductor	2.84%
75Ω Transformer	8.83%
50Ω Transformer	10.28%

Table A.6: Maximum relative error of the models

Printed by Tryckeriet i E-huset, Lund 2019

LUND
UNIVERSITY

Series of Master's theses
Department of Electrical and Information Technology
LU/LTH-EIT 2019-729
http://www.eit.lth.se